

# A new lipid-structured model to investigate the opposing effects of LDL and HDL on atherosclerotic plaque macrophages

Keith L Chambers<sup>a,\*</sup>, Mary R Myerscough<sup>b</sup>, Helen M Byrne<sup>a</sup>

<sup>a</sup>*Wolfson Centre for Mathematical Biology, Mathematical Institute, University of Oxford, Andrew Wiles Building, Radcliffe Observatory Quarter, Woodstock Road, Oxford, OX2 6GG, Oxfordshire, United Kingdom*

<sup>b</sup>*School of Mathematics and Statistics, University of Sydney, Carlaw Building, Eastern Avenue, Camperdown, Sydney, 2006, New South Wales, Australia*

---

## Abstract

Atherosclerotic plaques form in artery walls due to a chronic inflammatory response driven by lipid accumulation. A key component of the inflammatory response is the interaction between monocyte-derived macrophages and extracellular lipid. Although concentrations of low-density lipoprotein (LDL) and high-density lipoprotein (HDL) particles in the blood are known to affect plaque progression, their impact on the lipid load of plaque macrophages remains unexplored. In this paper, we develop a lipid-structured mathematical model to investigate the impact of blood LDL/HDL levels on plaque composition, and lipid distribution in plaque macrophages. A reduced subsystem, derived by summing the equations of the full model, describes the dynamics of biophysical quantities relating to plaque composition (e.g. total number of macrophages, total amount of intracellular lipid). We also derive a continuum approximation of the model to facilitate analysis of the macrophage lipid distribution. The results, which include time-dependent numerical solutions and asymptotic analysis of the unique steady state solution, indicate that plaque lipid content is sensitive to the influx of LDL relative to HDL capacity. The macrophage lipid distribution evolves in a wave-like manner towards an equilibrium profile which may be monotone decreasing, quasi-uniform or unimodal, attaining its maximum value at a non-zero lipid level. Our model also reveals that macrophage uptake may be severely impaired by lipid accumulation. We conclude that lipid accumulation in plaque macrophages may serve as a partial explanation for the defective uptake of apoptotic cells (efferocytosis) often reported in atherosclerotic plaques.

---

\*Corresponding author

*Email addresses:* [keith.chambers@maths.ox.ac.uk](mailto:keith.chambers@maths.ox.ac.uk) (Keith L Chambers),  
[mary.myerscough@sydney.edu.au](mailto:mary.myerscough@sydney.edu.au) (Mary R Myerscough), [helen.byrne@maths.ox.ac.uk](mailto:helen.byrne@maths.ox.ac.uk) (Helen M Byrne)

## 1. Introduction

Atherosclerosis is a chronic inflammatory disease that develops in the walls of major arteries [1, 2]. The condition begins when disturbed blood flow allows fatty compounds called lipids, which are carried upon low-density lipoprotein (LDL) particles, to enter the wall from the bloodstream [3]. The accumulation of lipid in the wall triggers an immune response that attracts monocyte-derived macrophages (MDMs) to the lesion. Macrophages are the dominant immune cell by number in atherosclerotic lesions [4]. They play a key role in disease progression by ingesting extracellular lipid in a process called *phagocytosis*. Over time the lesion may develop into an atherosclerotic plaque with a large core of extracellular lipid due to the persistent influx of lipid and the death of lipid-laden macrophages [5]. The rupture of such a plaque releases the lipid core material into the bloodstream, where it promotes blood clot formation. Blood clots can, in turn, block vessels in the heart and brain and induce myocardial infarction or stroke. The mechanisms that underpin macrophage lipid accumulation and extracellular lipid core formation remain an active area of research.

Macrophage lipid content is the product of phagocytosis and offloading events. Macrophages increase their lipid load by clearing the extracellular environment of LDL particles (which become modified upon entry and susceptible to macrophage ingestion [6]) and cellular debris via phagocytosis. In particular, macrophages phagocytose the lipid-rich contents of nearby dead macrophages. This includes lipid ingested by dead cells during their lifetime and also endogenous lipid contained in the membranes of cell corpses. Macrophages reduce their lipid burden by offloading lipid onto high-density-lipoprotein (HDL) particles, which also enter the lesion from the bloodstream. The lipoproteins LDL and HDL (which carry ‘bad’ and ‘good’ cholesterol respectively) therefore have opposing effects on macrophage lipid content. The impact of blood LDL/HDL levels on overall plaque composition and the distribution of lipid within the MDM population are well known but not completely understood.

The efficiency of macrophage phagocytosis and offloading is modulated by intracellular signalling [7, 8]). We note firstly that macrophages have a finite capacity for phagocytosis [7]. More specifically, experimental observations indicate that macrophages surrounded by an abundance of phagocytic targets dynamically regulate their rate of uptake according to

the available capacity. This behaviour is the result of physical limitations (e.g. finite cell size) and intracellular biochemical negative feedback signals. The study of Pinney et al. [9] indicates that the down-regulation of phagocytosis occurs on a rapid timescale ( $< 1$  hour). Hence, the reduction in macrophage phagocytic efficiency is likely to be commensurate with the current phagocytic load of a cell. Similarly, the efficiency of lipid offloading is also mediated by intracellular signalling [8]. The accumulation of cholesterol is known to activate transcription factors (e.g.  $Lxr\alpha$ ,  $Lxr\beta$ ) that upregulate the expression of transporters (e.g. ABCA1) which mediate cholesterol efflux to HDL particles. Taken together, the observations above indicate that, on average, heavily lipid-laden macrophages are less efficient at phagocytosis but more efficient at offloading than macrophages with a lesser lipid burden. Interestingly, many studies report that macrophage phagocytosis of apoptotic cells (termed *efferoctosis*) is defective in mid-to-late atherosclerotic plaques ([10, 11]). However, the extent to which this defective efferoctosis is attributable to the intrinsic down-regulation of phagocytosis due to lipid loading is not known.

There is growing interest in mathematical models of atherosclerosis [12, 13]. Many models partition the plaque macrophages into two sub-populations: those with a low lipid load (termed ‘macrophages’) and those that are heavily lipid-laden (termed ‘foam cells’) [14, 15, 16]. Lipid-dependent rates of phagocytosis and offloading are incorporated in this framework by assuming that only macrophages can ingest lipid and only foam cells can offload lipid (e.g. [15]). A more natural approach of representing lipid accumulation in plaque macrophages is to use a structured population model. Lipid-structured models for atherosclerosis have been developed by several authors [17, 18, 19, 20]. The models of Ford et al. [17], Chambers et al. [18] and Watson et al. [19] assume, for simplicity, that the rates of lipid uptake and offloading are independent of lipid load. The model of Meunier and Muller [20] accounts for an arbitrary lipid-dependent uptake rate of LDL, but does not account for uptake of cellular debris nor lipid offloading.

In this paper we present a new lipid-structured model for macrophage populations in atherosclerotic plaques. The primary aims of the study are to:

1. Investigate how blood LDL/HDL concentrations impact
  - (a) Plaque composition, and

- (b) The distribution of lipid in plaque macrophages;
2. Investigate the extent to which defective phagocytosis can be attributed to high lipid loads in macrophages.

The model is novel in that it (i) accounts for lipid-dependent rates of phagocytosis and offloading, (ii) explicitly tracks the amounts of extracellular lipid and HDL lipid capacity in the plaque, and (iii) is fundamentally based on a discrete structuring of the macrophage population. We also derive a continuum approximation of the discrete model to facilitate analysis of the macrophage lipid distribution in Section 3.3. The continuum approximation replaces the dynamical equations of the macrophage population with an advection-diffusion PDE subject to appropriate boundary conditions.

The remainder of the paper is structured as follows. Section 2 describes the model development, including the derivation of an ODE subsystem, non-dimensionalisation and treatment of model parameters. Section 3 contains the results of our model analysis. We present time-dependent numerical solutions and a steady state analysis of the ODE subsystem and macrophage lipid distribution. Finally, we summarise and discuss the implications of our results in Section 4, and present concluding remarks in Section 5.

## 2. Model development

In this section we present a lipid-structured model for MDM populations in early atherosclerotic lesions. We begin by outlining our assumptions and formulating the model as a coupled system of ODEs. We then show that the model admits a closed subsystem that can be solved and analysed independently of the full model. Finally we non-dimensionalise the model and outline our treatment of the dimensionless parameters.

### 2.1. Definitions and model statement

We assume for simplicity that macrophages take up and offload lipid in increments of mass  $\Delta a$ , and decompose the MDM population into a series of compartments according to lipid load. Specifically, we let  $m_j(t) \geq 0$  be the concentration of lesion MDMs with lipid content  $a_0 + j\Delta a$  at time  $t \geq 0$ . Here  $a_0$  is the mass of endogenous lipid that macrophages contain due to their membrane structure. The index  $j$  runs over integer values  $j = 0, 1, \dots, J$ , where  $J > 0$  defines

the macrophage lipid capacity. It follows that the maximal macrophage lipid content,  $\kappa$ , is given by  $\kappa = a_0 + J\Delta a$ . Finally, we denote the concentration of extracellular lipid by  $L(t)$ , and the total lipid capacity of the HDL particles in the lesion by  $H(t)$ , with  $H(t)$  proportional to the concentration of unloaded HDL particles by a factor  $\Delta a$ .

We propose that the MDM population evolves according to the following ODEs:

$$\frac{dm_0}{dt} = \sigma_M \frac{L}{L_c + L} - k_L L m_0 + k_H H \left(\frac{1}{J}\right) m_1 - (\beta + \gamma) m_0, \quad (1)$$

$$\begin{aligned} \frac{dm_j}{dt} = & k_L L \left[ \left(1 - \frac{j-1}{J}\right) m_{j-1} - \left(1 - \frac{j}{J}\right) m_j \right] \\ & + k_H H \left[ \left(\frac{j+1}{J}\right) m_{j+1} - \left(\frac{j}{J}\right) m_j \right] - (\beta + \gamma) m_j, \quad 1 \leq j \leq J-1, \end{aligned} \quad (2)$$

$$\frac{dm_J}{dt} = k_L L \left(\frac{1}{J}\right) m_{J-1} - k_H H m_J - (\beta + \gamma) m_J. \quad (3)$$

Equations (1)-(3) account for lipid uptake and offloading via the Law of Mass Action. Lipid uptake is modelled via the reaction:



Here we assume that the rate of lipid uptake decreases linearly with lipid content; it takes its maximal value  $k_L$  when  $j = 0$  and decreases to zero at  $j = J$ , so that macrophages cannot exceed  $J$  units of ingested lipid. Our treatment of lipid uptake is consistent with current understanding that macrophages have a finite capacity for phagocytosis, and that phagocytosis is mediated by intracellular signalling [7]. Lipid offloading is modelled via the reaction:



so that the rate constant for offloading increases linearly from zero at  $j = 0$  to its maximal value  $k_H H$  at  $j = J$ . This formulation is consistent with experimental evidence that intracellular accumulation of cholesterol leads to the up-regulation of transporters (e.g. ABCA1) that mediate the efflux of free cholesterol [8].

Equations (1)-(3) also account for macrophage recruitment, cell death and emigration. We assume that the rate at which macrophages are recruited to the lesion from the bloodstream can be described via a first-order Hill function in  $L(t)$ . The maximal recruitment rate is  $\sigma_M$  and half-maximal recruitment occurs at the value  $L = L_c$ . We assume that newly recruited macrophages carry only endogenous lipid (corresponding to  $j = 0$ ). Therefore, the recruitment

source term appears in equation (1) only. We further assume that all lesion macrophages undergo cell death at rate  $\beta > 0$ , and emigrate from the lesion at rate  $\gamma > 0$ .

We propose that the extracellular lipid dynamics are governed by:

$$\frac{dL}{dt} = \sigma_L + \beta \sum_{j=0}^J (a_0 + j\Delta a) m_j - k_L \Delta a L \sum_{j=0}^J \left(1 - \frac{j}{J}\right) m_j - \delta_L L. \quad (6)$$

In equation (6) we assume that extracellular lipid is sourced from the bloodstream at rate  $\sigma_L$ , due to LDL particle influx. We assume further that the lipid content of dying macrophages is transferred to the extracellular space, giving rise to the second source term in equation (6). Recall that  $\kappa = a_0 + J\Delta a$  is the maximal macrophage lipid content. The third term accounts for lipid removal from the extracellular space by macrophages, at a rate proportional to  $k_L$  (see reaction (4)). Finally, we assume that extracellular lipid is lost to non-MDM interactions (e.g. uptake by the self-renewing population of tissue-resident cells [21]) at a constant rate  $\delta_L$ , which we will assume to be small.

We model the HDL dynamics via the equation:

$$\frac{dH}{dt} = \sigma_H - k_H \Delta a H \sum_{j=0}^J \left(\frac{j}{J}\right) m_j - \delta_H H. \quad (7)$$

The ODE (7) assumes that HDL lipid capacity is sourced at rate,  $\sigma_H$ , due to a constant influx of unloaded HDL particles from the bloodstream, and lost to macrophage offloading at a rate proportional to  $k_H$  (according to the reaction (5)). The final term accounts for loss of unloaded HDL to non-MDM interactions (e.g. lipid-loading by tissue-resident cells) at the constant rate  $\delta_H$ , which we will assume to be small.

We close equations (1)-(3), (6) and (7) by imposing the following initial conditions:

$$m_j(0) = 0, \quad j = 0, 1, \dots, J, \quad L(0) = 0, \quad H(0) = 0. \quad (8)$$

These equations assume that the lesion is initially devoid of macrophages, extracellular lipid and HDL. We provide a schematic representation of the model in Figure 1.

## 2.2. An ODE subsystem

A closed ODE subsystem can be derived from equations (1)-(8) by considering the total concentration of lesion macrophages,  $M(t)$ , and the total concentration of intracellular lipid,

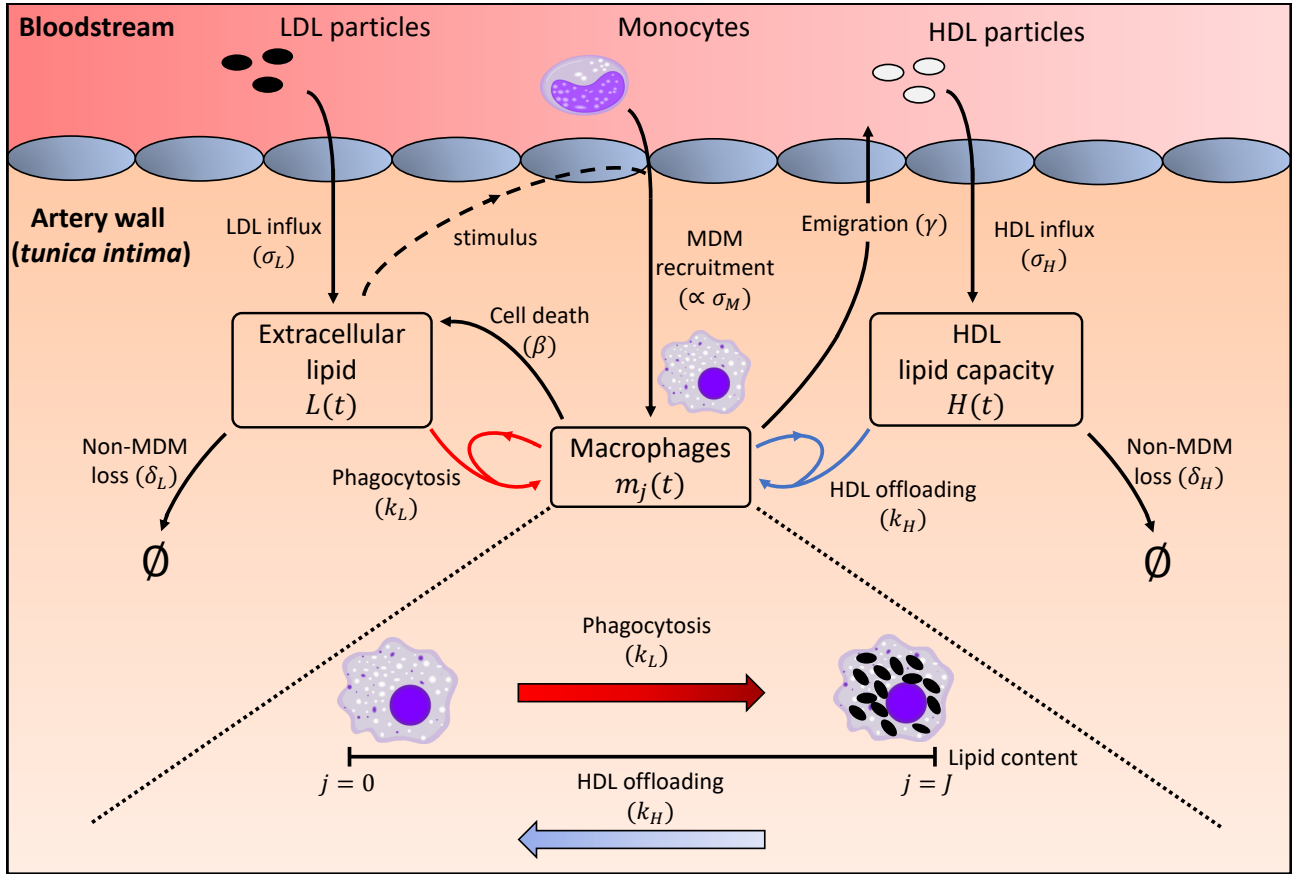


Figure 1: **Schematic representation of the model** (1)-(8). We track extracellular lipid,  $L(t)$ , the lipid capacity of the HDL particles,  $H(t)$ , and the number of macrophages,  $m_j(t)$ , with lipid content  $a_0 + j\Delta a$  ( $j = 0, 1, \dots, J$ ). Note the opposing effect of LDL vs HDL particle influx on macrophage lipid content. The LDL influx provides a source of extracellular lipid and hence promotes increases to macrophage lipid load via phagocytosis. By contrast, the entry of HDL promotes decreases in macrophage lipid content via offloading.

$A_M(t)$ , where,

$$M(t) := \sum_{j=0}^J m_j(t), \quad A_M(t) = \sum_{j=0}^J (a_0 + j\Delta a)m_j(t). \quad (9)$$

Summing equations (1)-(3), we find that  $M(t)$  evolves according to the equation:

$$\frac{dM}{dt} = \sigma_M \frac{L}{L_c + L} - (\beta + \gamma)M. \quad (10)$$

Equation (10) reflects our assumptions that lesion macrophages are sourced from the bloodstream at rate which is an increasing, saturating function of the extracellular lipid load,  $L(t)$ , and removed via apoptosis and emigration at constant rates  $\beta$  and  $\gamma$  respectively. By multiplying each of equations (1)-(3) by the corresponding index  $j$  and then summing, it is straightforward to show that the dynamics of  $A_M(t)$  are given by:

$$\frac{dA_M}{dt} = a_0\sigma_M \frac{L}{L_c + L} + \frac{k_L \Delta a}{\kappa - a_0}(\kappa M - A_M)L - \frac{k_H \Delta a}{\kappa - a_0}(A_M - a_0M)H - (\beta + \gamma)A_M. \quad (11)$$

Equation (11) shows how intracellular lipid levels increase due to the influx of macrophages from the bloodstream and uptake of extracellular lipid. We note that the rate of uptake across the macrophage population is proportional to the quantity  $\kappa M(t) - A_M(t)$ , which represents the lipid capacity of the macrophage population at time  $t$ . Intracellular lipid is removed to offloading to HDL, apoptosis and emigration. The rate of lipid offloading across the macrophage population is proportional to  $A_M(t) - a_0 M(t)$ , which is the total amount of ingested lipid (i.e. non-endogenous lipid) in the macrophage population.

Using definitions (9) we simplify equations (6) and (7) to obtain:

$$\frac{dL}{dt} = \sigma_L + \beta A_M - \frac{k_L \Delta a}{\kappa - a_0}(\kappa M - A_M)L - \delta_L L, \quad (12)$$

$$\frac{dH}{dt} = \sigma_H - \frac{k_H \Delta a}{\kappa - a_0}(A_M - a_0 M)H - \delta_H H. \quad (13)$$

We note that equations (10)-(13) define a closed subsystem for  $M$ ,  $A_M$ ,  $L$  and  $H$ , which we solve subject to the following initial conditions:

$$M(0) = 0, \quad A_M(0) = 0, \quad L(0) = 0, \quad H(0) = 0, \quad (14)$$

which we obtain from equations (8).

### 2.3. Non-dimensionalisation

We recast the model in terms of the following dimensionless variables:

$$\begin{aligned}\hat{t} &:= \beta t, & \hat{m}_j(\hat{t}) &:= \frac{\beta}{\sigma_M} m_j(t), & \hat{M}(\hat{t}) &:= \frac{\beta}{\sigma_M} M(t), \\ \hat{L}(\hat{t}) &:= \frac{\beta}{a_0 \sigma_M} L(t), & \hat{A}_M(\hat{t}) &:= \frac{\beta}{a_0 \sigma_M} A_M(t), & \hat{H}(\hat{t}) &:= \frac{\beta}{a_0 \sigma_M} H(t)\end{aligned}\tag{15}$$

Under this rescaling, time is measured in units of average macrophage lifespan,  $\beta^{-1}$ , and the macrophage concentrations are normalised with respect to  $\frac{\sigma_M}{\beta}$ , the maximal concentration of MDMs supplied to the lesion per macrophage lifespan. The lipid concentrations  $L(t)$ ,  $A_M(t)$  and the HDL lipid capacity,  $H(t)$ , are scaled with respect to  $a_0 \sigma_M / \beta$ , which is the maximal concentration of endogenous lipid entering the lesion per macrophage lifespan.

We also define a number of dimensionless parameters in Table 1. The first two parameters,  $\hat{\kappa}$  and  $J$ , are lipid ratios. The remaining parameters pertain to the model kinetics:  $\hat{\sigma}_L$  and  $\hat{\sigma}_H$ , determine the rates at which LDL and HDL respectively enter the lesion;  $\hat{k}_L$  is the dimensionless phagocytosis rate per unit extracellular lipid;  $\hat{k}_H$  is the dimensionless offloading rate per unit HDL capacity;  $\hat{L}_c$  is the value of  $\hat{L}(\hat{t})$  at which macrophage recruitment is half-maximal;  $\hat{\gamma}$  is the dimensionless emigration rate;  $\hat{\delta}_L$  is the dimensionless rate of extracellular lipid loss to non-MDM effects; and  $\hat{\delta}_H$  determines the rate of unloaded HDL loss to non-MDM effects.

By applying the scaling (15) and the definitions of Table 1, and dropping the hats for notational convenience, we obtain the following dimensionless ODEs for the macrophage dynamics:

$$\frac{dm_0}{dt} = \frac{L}{L_c + L} - k_L J L m_0 + k_H H m_1 - (1 + \gamma) m_0,\tag{16}$$

$$\begin{aligned}\frac{dm_j}{dt} &= k_L L [(J - j + 1) m_{j-1} - (J - j) m_j] \\ &\quad + k_H H [(j + 1) m_{j+1} - j m_j] - (1 + \gamma) m_j, \quad 1 \leq j \leq J - 1,\end{aligned}\tag{17}$$

$$\frac{dm_J}{dt} = k_L L m_{J-1} - k_H H J m_J - (1 + \gamma) m_J,\tag{18}$$

and the following closed subsystem for  $M$ ,  $A_M$ ,  $L$  and  $H$ :

$$\frac{dM}{dt} = \frac{L}{L_c + L} - (1 + \gamma) M,\tag{19}$$

$$\frac{dA_M}{dt} = \frac{L}{L_c + L} + k_L (\kappa M - A_M) L - k_H (A_M - M) H - (1 + \gamma) A_M,\tag{20}$$

$$\frac{dL}{dt} = \sigma_L + A_M - k_L (\kappa M - A_M) L - \delta_L L,\tag{21}$$

$$\frac{dH}{dt} = \sigma_H - k_H (A_M - M) H - \delta_H H.\tag{22}$$

Dimensionless parameter	Definition	Physical interpretation
$\hat{\kappa}$	$\frac{\kappa}{a_0}$	Ratio of the maximum macrophage lipid content to endogenous lipid content
$J$	$\frac{\kappa - a_0}{\Delta a}$	Ratio of macrophage lipid capacity to the increment of lipid uptake/offloading
$\hat{\sigma}_L$	$\frac{\sigma_L}{a_0 \sigma_M}$	Influx of LDL lipid relative to maximal influx of endogenous lipid
$\hat{\sigma}_H$	$\frac{\sigma_H}{a_0 \sigma_M}$	Influx of HDL capacity relative to maximal influx of endogenous lipid
$\hat{k}_L$	$\frac{k_L \Delta a a_0 \sigma_M}{\beta^2 (\kappa - a_0)}$	Dimensionless rate of lipid uptake per unit of extracellular lipid
$\hat{k}_H$	$\frac{k_H \Delta a a_0 \sigma_M}{\beta^2 (\kappa - a_0)}$	Dimensionless rate of lipid offloading per unit of HDL capacity
$\hat{L}_c$	$\frac{L_c \beta}{a_0 \sigma_M}$	Value of $\hat{L}$ for which macrophage recruitment is half-maximal
$\hat{\gamma}$	$\frac{\gamma}{\beta}$	Dimensionless rate of emigration
$\hat{\delta}_L$	$\frac{\delta_L}{\beta}$	Dimensionless rate of extracellular lipid loss to non-MDM interactions
$\hat{\delta}_H$	$\frac{\delta_H}{\beta}$	Dimensionless rate of unloaded HDL loss to non-MDM interactions

Table 1: The dimensionless parameters that appear in equations (16)-(21).

The initial conditions used to close equations (16)-(22) are unchanged and stated here for completeness:

$$m_j(0) = 0, \quad j = 0, 1, \dots, J, \quad M(0) = A_M(0) = L(0) = H(0) = 0. \quad (23)$$

In their dimensionless forms,  $M(t)$  and  $A_M(t)$  are related to the functions  $m_j(t)$  via the summations:

$$M(t) = \sum_{j=0}^J m_j(t), \quad A_M(t) = M(t) + \frac{\kappa - 1}{J} \sum_{j=0}^J j m_j(t). \quad (24)$$

#### 2.4. Model parameter estimation

In what follows, unless stated otherwise, we use the following dimensionless parameter values in our numerical simulations:

$$\hat{\kappa} = 30, \quad J = 100, \quad \hat{k}_L = \hat{k}_H = 1, \quad \hat{\gamma} = 0.25, \quad \hat{L}_c = 1, \quad \hat{\delta}_L = \hat{\delta}_H = 0.01. \quad (25)$$

The influx ratios  $\hat{\sigma}_L$  and  $\sigma_H$  are varied over a range of positive values. We briefly justify these choices below.

The estimate for  $\hat{\kappa} = \kappa/a_0$  is based on the experimental results presented in [22]. Ford *et al.* measured the rate at which macrophages uptake endogenous lipid from apoptotic cells and found that, even when extracellular lipid was in abundance, macrophages did not attain a lipid load exceeding  $\sim 30a_0$ .

The average unit of lipid exchange,  $\Delta a$ , is likely to be much smaller than the macrophage capacity,  $\kappa - a_0$ . Indeed, the largest increment of lipid exchange is likely to be due to apoptotic cell uptake (efferocytosis) or necrotic cell uptake, processes which are often reported to occur via piecemeal uptake or via nibbling respectively [23, 24]. Hence, a possible upper bound for  $\Delta a$  in early atherosclerotic lesions is the endogenous lipid content:  $\Delta a \lesssim a_0$ . In light of our estimate for  $\kappa$ , it follows that  $J^{-1} = \frac{\Delta a}{\kappa - a_0} \lesssim 0.03$ .

The estimate for  $\hat{\gamma} = \gamma/\beta$  is based on a macrophage death rate of  $\beta = 0.05 \text{ h}^{-1}$  and an emigration rate of  $\gamma = 0.013 \text{ h}^{-1}$ . The stated death rate is the half-maximal value of the apoptosis rate reported in [25], where the authors fit an ODE model to *in vitro* data for macrophage lipid uptake. Thon *et al.* assume that the death rate increases with lipid content (by contrast we assume a constant death rate). Since our model distinguished between

newly recruited and lipid-laden macrophages, we use the half-maximal rate rather than the maximal rate. The stated emigration rate is intermediate between the 12.6% transmigration rate reported in [26] and the 20h residence time reported in [27].

The remaining parameters are difficult to estimate due to the current lack of quantitative *in vivo* data. In the absence of such data, we fix  $\hat{k}_L = \hat{k}_H = 1$ . These values ensure that macrophage phagocytosis and offloading are comparable and occur on the same timescale as the macrophage lifespan. We also fix  $\delta_L = \delta_H = 0.01$  so that loss of extracellular lipid and unloaded HDL to non-MDM interactions is small relative to MDM phagocytosis and offloading. This assumption is consistent with observations that the number of tissue-resident cells in atherosclerotic plaques is dominated by the number of recruited MDMs [21]. Finally, we set  $\hat{L}_c = 1$  so MDM recruitment also occurs on the  $t = \mathcal{O}(1)$  macrophage lifespan timescale. The LDL and HDL influx ratios,  $\hat{\sigma}_L$  and  $\hat{\sigma}_H$ , are likely to vary significantly between individuals since blood cholesterol levels depend sensitively on lifestyle factors such as diet [28]. Nonetheless, the estimates in [25] indicate that  $\hat{\sigma}_L$  and  $\sigma_H$  are likely to be  $\mathcal{O}(1)$  quantities.

### 3. Results

In this section we explore the behaviour of equations (16)-(23). We present time-dependent numerical solutions of the full model in Subsection 3.1. We then conduct a steady state analysis of the subsystem (19)-(21) in Subsection 3.2. Finally, in Subsection 3.3, we characterise the macrophage lipid distribution by deriving and then exploiting a continuum approximation of equations (16)-(18).

#### 3.1. Model dynamics

We use Wolfram Mathematica's *NDSolve* routine to generate numerical solutions across a range of values of the influx parameters  $\sigma_L$  and  $\sigma_H$ . The dynamics of the ODE subsystem (19)-(23) are shown in Figure 2. At early times,  $t \lesssim 0.25$  (see insets of Figs. 2d, g), we observe quasi-linear growth in  $L(t)$  and  $H(t)$ , which reflects LDL and HDL infiltrating a lesion that is initially devoid of monocyte-derived macrophages. The initial rise in  $L(t)$  drives a rapid increase in  $M(t)$  and  $A_M(t)$  as macrophages are recruited to the lesion from the blood. The growth in  $L(t)$  then slows substantially for  $0.5 \lesssim t \lesssim 1$  due to macrophage phagocytosis. We note that this initial wave of phagocytosis is sufficient to cause  $L(t)$  to decrease in many of the

cases shown, which indicates that the rate of phagocytosis exceeds the rate of LDL entry to the tissue during this period. For  $1 \lesssim t \lesssim 2$ , growth in  $H(t)$  slows, indicating that at this stage the macrophage population has ingested enough lipid for offloading to substantially impact the amount of unloaded HDL in the lesion. Indeed for sufficiently large values of  $(\sigma_L - \sigma_H)$  (see cases b,c,e,f,h,i), intracellular lipid loads are sufficiently large that offloading causes  $H(t)$  to peak and decrease thereafter. We note also that macrophage cell death gives rise to a secondary increase in  $L(t)$  in these cases during this time period; the increase in extracellular lipid due to cell death exceeds the loss due to phagocytosis for sufficiently large values of  $\sigma_L$  relative to  $\sigma_H$ . Finally, we observe that  $M(t)$ ,  $A_M(t)$ ,  $L(t)$  and  $H(t)$  evolve to nonzero equilibrium values as  $t \rightarrow \infty$ .

The numerical solutions suggest that plaque lipid content at equilibrium is more sensitive to the relative influx of LDL to HDL,  $(\sigma_L - \sigma_H)$ , than to the individual influx rates  $\sigma_L$  and  $\sigma_H$ . Indeed, when  $\sigma_L - \sigma_H = 2$  the trajectories of  $A_M(t)$  and  $L(t)$  are indistinguishable for  $t \gtrsim 4$  (see Fig.2, cases c,f,i). We note further that larger values of  $(\sigma_L - \sigma_H)$  give rise to larger increases in  $A_M(t)$  than in  $L(t)$  for the parameter values used in Figure 2. That is, increases to the relative influx of LDL to HDL yield greater changes in the macrophage lipid burden than the amount of extracellular lipid for these parameter values. These trends will be explored in more detail in Section 3.2.

The dynamics of the macrophage lipid distribution,  $m_j(t)$ ,  $j = 0, 1, \dots, J$ , are shown in Figure 3. We see that, over time,  $m_j(t)$  evolves in a wave-like manner towards a non-zero equilibrium. The wavefront proceeds from  $j = 0$  at  $t = 0$  to  $j = j_c \in (0, J]$  as  $t \rightarrow \infty$ . We note, however, that the wavefront may change direction at later times (e.g. case a in Fig.3). This is likely due to offloading to HDL, given the dominance of  $H(t)$  for these parameter values (see Fig.2a).

The lipid distribution  $m_j$  adopts several qualitatively distinct profiles at equilibrium. The equilibrium profile may be monotone decreasing in  $j$ , and may be convex (as in case g) or concave (cases d and h); it may have a quasi-uniform profile (case e) or a peaked profile (cases a,b,c,f and i). The simulation results presented in Figure 3 suggest that the location of the wavefront at steady state is sensitive to the difference  $(\sigma_L - \sigma_H)$ . However, the geometric features of the profile (e.g. existence of a local maximum) seem to depend on the individual

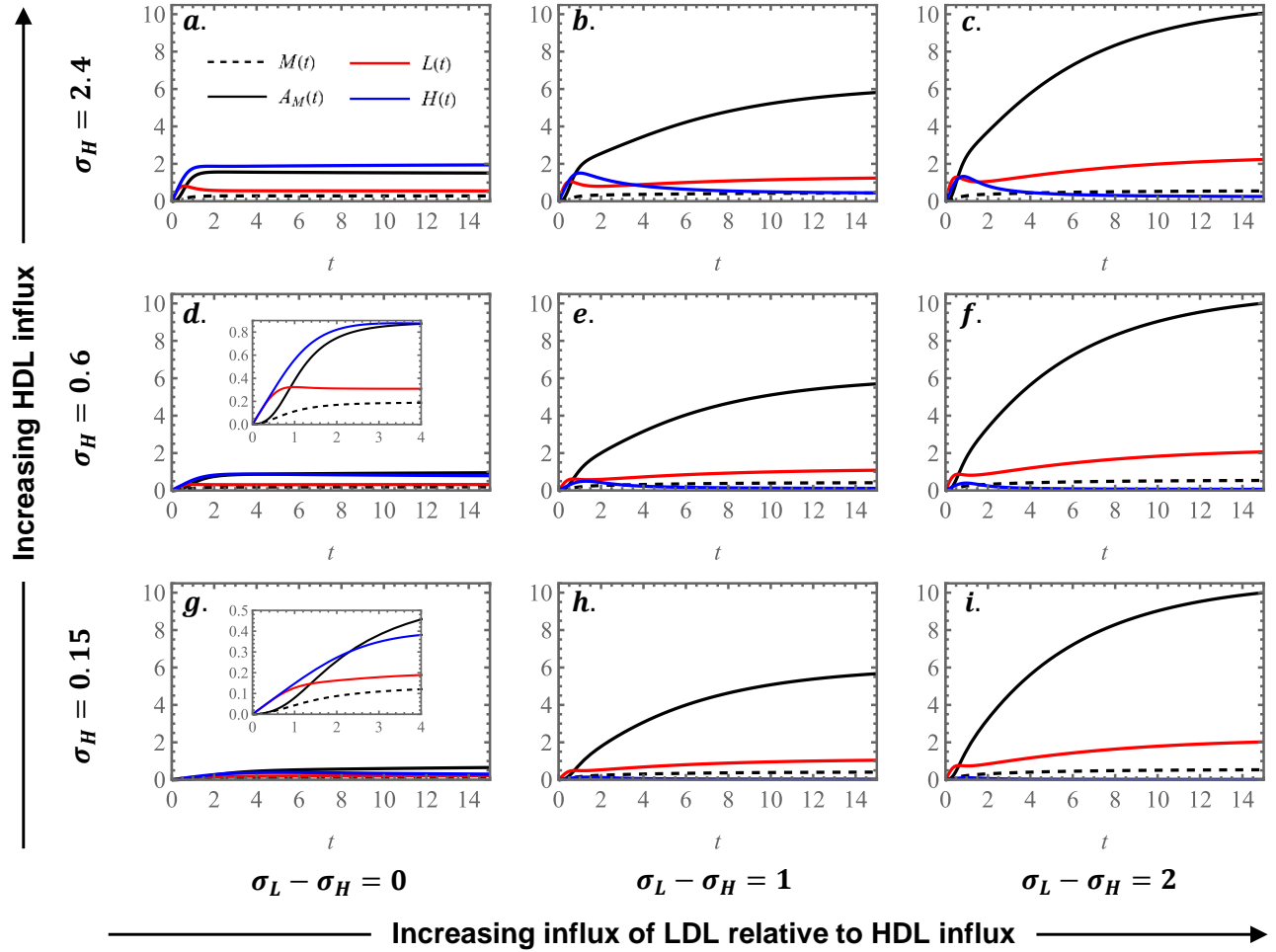


Figure 2: Series of plots showing how plaque composition against time for different rates of LDL/HDL entry. The time dynamics of the macrophage population,  $M$ , intracellular lipid content,  $A_M$ , extracellular lipid content,  $L$  and HDL capacity for lipid,  $H$ , are presented for a range of values of the parameters  $\sigma_L$  and  $\sigma_H$ . We consider the cases  $\sigma_H = 0.15, 0.6$  and  $2.4$  in the top, middle and bottom rows respectively. The LDL influx,  $\sigma_L$ , is increased from  $\sigma_H$  to  $\sigma_H + 1$  and finally  $\sigma_H + 2$  from left to right. The remaining parameter values are given in equation (25).

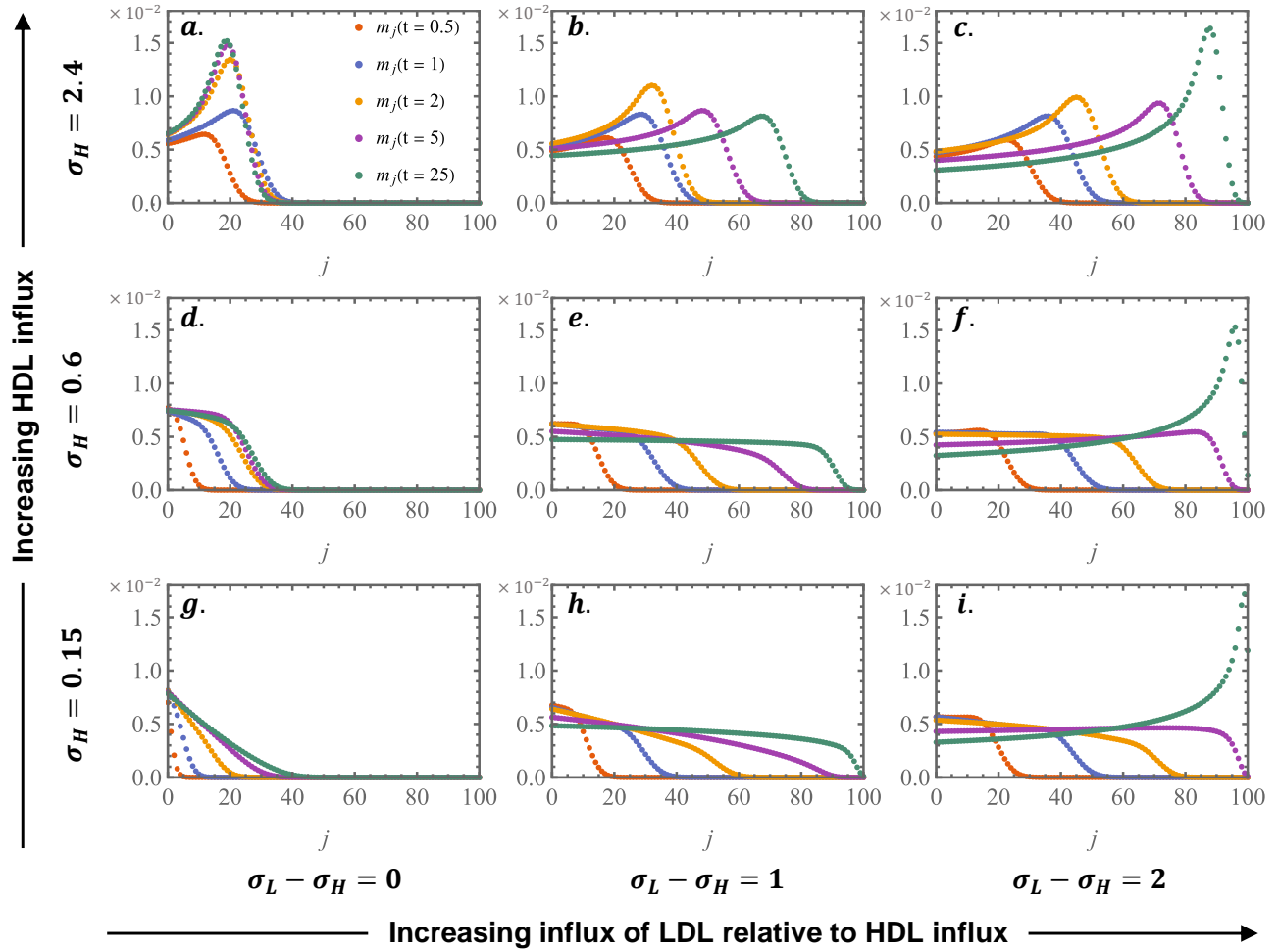


Figure 3: **Dynamics of the macrophage lipid distribution for different rates of LDL and HDL influx.** The distribution functions,  $m_j(t)$ ,  $j = 0, 1, \dots, J$ , are plotted against  $j$  at the time values  $t = 0.5, 1, 2, 5$  and  $25$  (approximately steady state). We consider the same values of  $\sigma_L$  and  $\sigma_H$  as in Figure 2. The remaining parameters are set according to equation (25).

magnitudes of  $\sigma_L$  and  $\sigma_H$ . For instance, the spiked profile can manifest with low (e.g. case a), intermediate (e.g. case b) or high (e.g. case c) lipid loads. We study the equilibrium lipid distribution in more depth in Section 3.3.

Before proceeding to the steady state analysis, we pause to define two quantities which help to summarise the model behaviour:

$$\mu(t) := \frac{A_M(t) - M(t)}{(\kappa - 1)M(t)}, \quad f(t) := \frac{A_M(t)}{A_M(t) + L(t)}. \quad (26)$$

Both variables are normalised such that  $0 \leq \mu(t), f(t) \leq 1$ . The ratio  $\mu(t)$  represents the average macrophage lipid burden, relative to the capacity for ingested lipid. Since

$$\mu = 1 - \frac{k_L(\kappa M - A_M)L}{k_L(\kappa M - M)L}, \quad (27)$$

we note that another interpretation for  $\mu$  is the fractional decrease in the phagocytosis rate of the macrophage population due to the lipid load at time  $t$ . The ratio  $f(t)$  is the fraction of lipid in the lesion that is contained within the macrophage population.

The dynamics of  $\mu(t)$  and  $f(t)$  are shown in Figure 4 for  $\sigma_H = 1$  and  $\sigma_L = 0.75, 1.5, 3, 6$  and  $12$ . Both variables tend to non-zero steady state values at long times:  $\mu \rightarrow \mu^*$  and  $f \rightarrow f^*$  as  $t \rightarrow \infty$ . We observe that as  $\sigma_L$  increases,  $\mu^*$  increases towards  $\mu^* \rightarrow 1^-$ , which corresponds to a plaque with macrophage lipid loads at capacity and, consequently, 100% defective phagocytosis. By contrast,  $f^*$  depends non-monotonically on  $\sigma_L$ , attaining its largest value,  $f^* \approx 0.8$ , when  $1.5 \lesssim \sigma_L \lesssim 3$ . In order to understand these trends and those described above, we turn now to the steady state analysis.

### 3.2. Steady state analysis of subsystem (19)-(23)

Let  $M^*$ ,  $A_M^*$ ,  $L^*$  and  $H^*$  denote the steady values of the corresponding dependent variables. Expressions for these quantities can be found by setting the time derivatives to zero in equations (19)-(21). We find that  $M^*$ ,  $A_M^*$  and  $H^*$  can be expressed in term of  $L^*$ :

$$\begin{aligned} M^* &= \frac{L^*}{(1 + \gamma)(L_c + L^*)}, & A_M^* &= \frac{k_L \kappa (L^*)^2 - \sigma_L (1 + \gamma)(L^* + L_c)}{(1 + \gamma)(1 + k_L L^*)(L^* + L_c)}, \\ H^* &= \frac{\sigma_H}{\delta_H + k_H(A_M^* - M^*)}, \end{aligned} \quad (28)$$

and that  $L^*$  solves a quintic equation:

$$c_5(L^*)^5 + c_4(L^*)^4 + c_3(L^*)^3 + c_2(L^*)^2 + c_1 L^* + c_0 = 0. \quad (29)$$

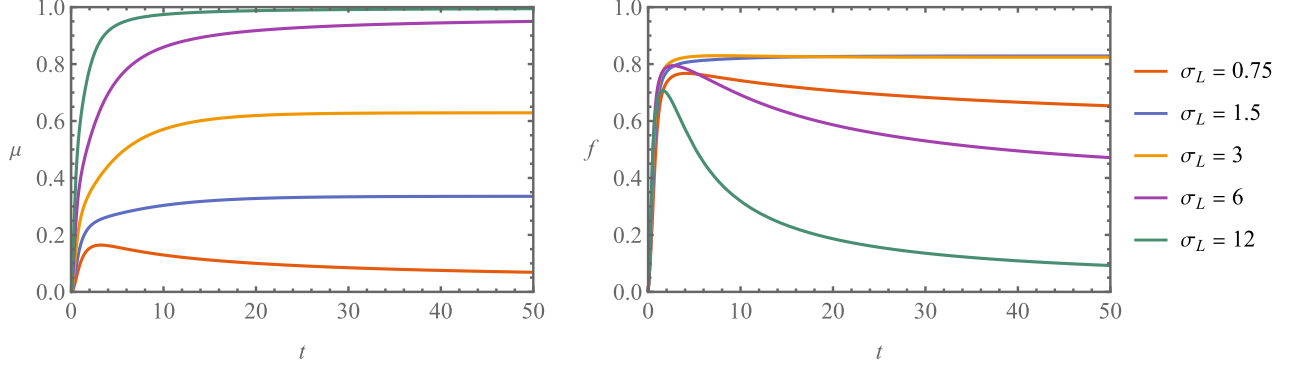


Figure 4: **Fractional decrease in phagocytosis rate due to lipid accumulation,  $\mu(t)$ , and proportion of lesion lipid that is intracellular,  $f(t)$ .** The quantities  $\mu(t)$  and  $f(t)$ , defined in equations (26), are plotted for the cases  $\sigma_L = 0.75, 1.5, 3, 6$  and  $12$  with  $\sigma_H = 1$ . We set the remaining parameters according to equation (25).

The coefficients  $c_i$ ,  $i = 1, \dots, 5$  are complicated combinations of the model parameters. Their expressions are given in Appendix A. We note that physically realistic steady state solutions must satisfy  $A_M^* \geq M^*$  so that macrophage lipid content is not less than the endogenous lipid content. Re-writing this condition using the expressions for  $A_M^*$  and  $M^*$  in equations (28) supplies the following inequality for  $L^*$ :

$$L^* \geq \frac{1}{2(k_L(\kappa - 1) + \delta_L(1 + \gamma))} \left[ (1 - (1 + \gamma)(\sigma_L - \delta_L L_c)) + \sqrt{(1 - (1 + \gamma)(\sigma_L - \delta_L L_c))^2 - 4(k_L(\kappa - 1) + \delta_L(1 + \gamma))(1 + \gamma)\sigma_L L_c} \right] \quad (30)$$

$$=: L_{\min}^*.$$

Hence, we seek positive solutions of the quintic (29) which satisfy inequality (30).

We used the Wolfram Mathematica routine *NSolve* to determine the positive solutions of equation (29) as  $\sigma_L$  varies. The results, presented in Figure 5a, show that for fixed values of  $\sigma_L$  polynomial (29) admits a unique physically realistic solution (with  $L^* \geq L_{\min}^*$ ). Further,  $L^*$  increases continuously with  $\sigma_L$  and the solution branch can be decomposed into two main segments. On the left segment ( $0 \leq \sigma_L \lesssim 0.8$  in Fig.5)  $L^*$  increases slowly with  $\sigma_L$  and is well-approximated by  $L_{\min}^*$ . This regime corresponds to an HDL-dominant plaque where macrophage lipid loads are minimal ( $A_M^* \approx M^*$ ) due to efficient offloading. In this regime, increasing LDL influx,  $\sigma_L$ , has little effect on extracellular lipid accumulation at equilibrium because macrophages rapidly offload the lipid they ingest and, therefore, only contribute their

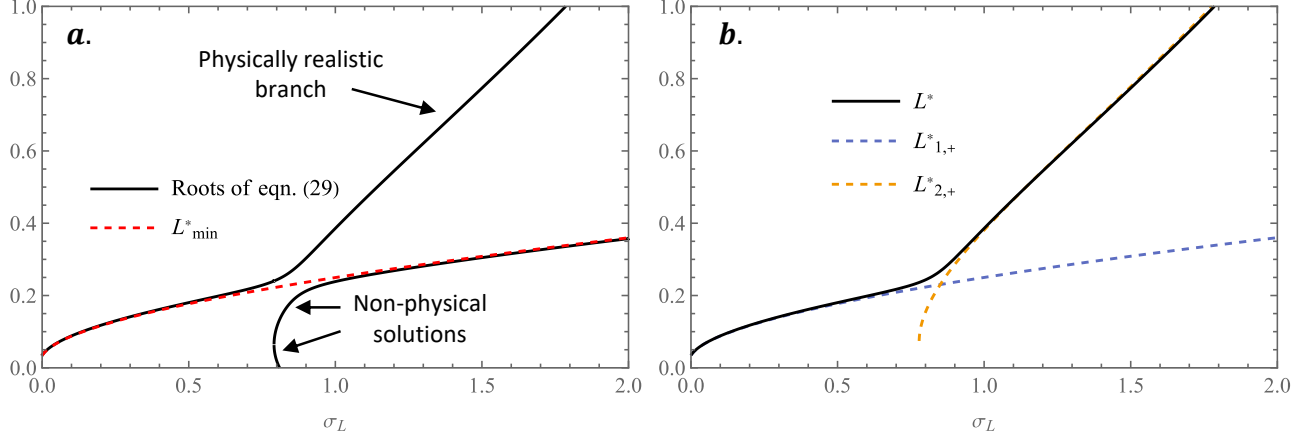


Figure 5: **Identifying and approximating the physical solution,  $L^*$ , of the polynomial (29).** The left plot shows the positive solutions of equation (29) as the LDL influx,  $\sigma_L$ , is varied. There is only one physically realistic solution which satisfies  $L^* \geq L^*_{\min}$ . The right plot shows how the left and right segments of this physical solution are approximated by the asymptotic solutions,  $L^*_{1,+}$  and  $L^*_{2,+}$ , respectively. We use  $\sigma_H = 1$  and set the remaining parameter values according to equation (25).

endogenous lipid content to the extracellular environment upon death. For large values of  $\sigma_L$  ( $\sigma_L \gtrsim 0.8$  in Fig.5)  $L^*$  increases more rapidly with  $\sigma_L$ . For these plaques the LDL influx,  $\sigma_L$ , is sufficiently large to impact the quantity of unloaded HDL in the lesion at steady state.

While a closed-form expressions for  $L^*$  does not exist in full generality, we can approximate the individual segments of  $L^*$  via asymptotic analysis. Specifically, we seek approximate solutions to the polynomial (29) in the limit  $\delta_L \sim \delta_H \ll 1$ . Biologically, this corresponds to a regime in which loss of extracellular lipid and unloaded HDL to non-MDM interactions is negligible. It is possible to show that at leading order (see Appendix A), the coefficients scale as:  $c_0, \dots, c_4 = \mathcal{O}(1)$  and  $c_5 = \mathcal{O}(\delta_L, \delta_H)$ , so that equation (29) can be interpreted as a singular perturbation problem. We first consider the “outer” problem by setting  $\delta_L, \delta_H \rightarrow 0$  in equation (29). By factorising the resulting quartic polynomial into two quadratic equations for  $L^*$ , we arrive at the following solutions:

$$L^*_{1,\pm} := \frac{\gamma\sigma_L + \sigma_L + 1 \pm \sqrt{4(\gamma+1)(\kappa-1)L_c k_L \sigma_L + (\gamma\sigma_L + \sigma_L + 1)^2}}{2(\kappa-1)k_L}, \quad (31)$$

$$L^*_{2,\pm} := \frac{-b_1 \pm \sqrt{b_1^2 - 4b_0 b_2}}{2b_2}, \quad (32)$$

where the constants  $b_0, b_1$  and  $b_2$  of  $L_{2,\pm}^*$  are given by:

$$\begin{aligned} b_0 &:= L_c(1 + \gamma)[(1 + \gamma)\sigma_L - \sigma_H], \\ b_1 &:= (\gamma + 1)[1 + k_L L_c(\sigma_L - \sigma_H) + (1 + \gamma)\sigma_L - \sigma_H], \\ b_2 &:= k_L[(1 + \gamma)(1 + \sigma_L - \sigma_H) - \gamma\kappa]. \end{aligned} \tag{33}$$

The remaining root is negative and scales as  $L_0^* = \mathcal{O}(\delta_L^{-1}, \delta_H^{-1})$ .

In Figure 5b we show how the solutions  $L_{1,+}^*$  and  $L_{2,+}^*$  change as  $\sigma_L$  varies. We note that these expressions are good approximations for the left and right segments of  $L^*$  respectively. We note further that  $L_{\min}^*$  reduces to  $L_{1,+}^*$  in the limit  $\delta_L \rightarrow 0$ , which indicates that  $L_{1,+}^*$  corresponds to a regime where  $A_M^* = M^* + \mathcal{O}(\delta_L, \delta_H)$ . Substituting this result into equations (28) shows that  $H^* = \mathcal{O}(\delta_L^{-1}, \delta_H^{-1})$  at leading order, confirming that the slower increase with  $\sigma_L$  on the left branch  $L_{1,+}^*$  is due to rapid offloading to HDL. The expression for  $L_{2,+}^*$  is more complicated and difficult to interpret. However, we note that the coefficients (33) which define  $L_{2,+}^*$  only depend on the influx parameters  $\sigma_L$  and  $\sigma_H$  through the combinations  $\sigma_L - \sigma_H$  and  $(1 + \gamma)\sigma_L - \sigma_H$ . This reinforces the notion that  $L^*$  is sensitive to the relative influx of LDL and HDL.

In Figure 6, we use the expressions (28) with the numerical solution for  $L^*$  in equation (29) to show how plaque composition at equilibrium changes as both  $\sigma_L$  and  $\sigma_H$  vary. We find that  $M^*$ ,  $A_M^*$  and  $L^*$  each increase with  $\sigma_L$  and decrease with  $\sigma_H$ . By contrast,  $H^*$  decreases with  $\sigma_L$  and increases with  $\sigma_H$ . We note that the approximately linear contours, which feature in all four plots, indicate that the dependent variables are sensitive to the difference  $\sigma_L - \sigma_H$ . This suggests that the relative influx of LDL lipid to HDL capacity not only determines  $L^*$  (as indicated by the asymptotics), but plaque composition more generally. When  $\sigma_L - \sigma_H \lesssim 0$  (top left in plots of Fig.6), the plaque is HDL-dominant ( $H^* > 25$ ) with low quantities of lipid ( $A_M^*, L^*$ ) and a small macrophage population ( $M^*$ ). For  $0 \lesssim \sigma_L - \sigma_H \lesssim 5$  the plaque contains intermediate amounts of macrophages, lipid and HDL capacity. Finally, when  $\sigma_L - \sigma_H \gtrsim 5$  the plaque is dominated by extracellular lipid ( $L^* > 25$ ). In this regime, HDL capacity is exhausted ( $H^* \approx 0$ ) and macrophage lipid loads are near capacity ( $A_M^* \approx \kappa M^*$ ) so that increases to the LDL lipid influx relative to HDL capacity, ( $\sigma_L - \sigma_H$ ), directly increase the amount of extracellular lipid at steady state ( $L^*$ ).

We further explore plaque composition in Figure 7 where we focus on  $\mu^*$ , the average

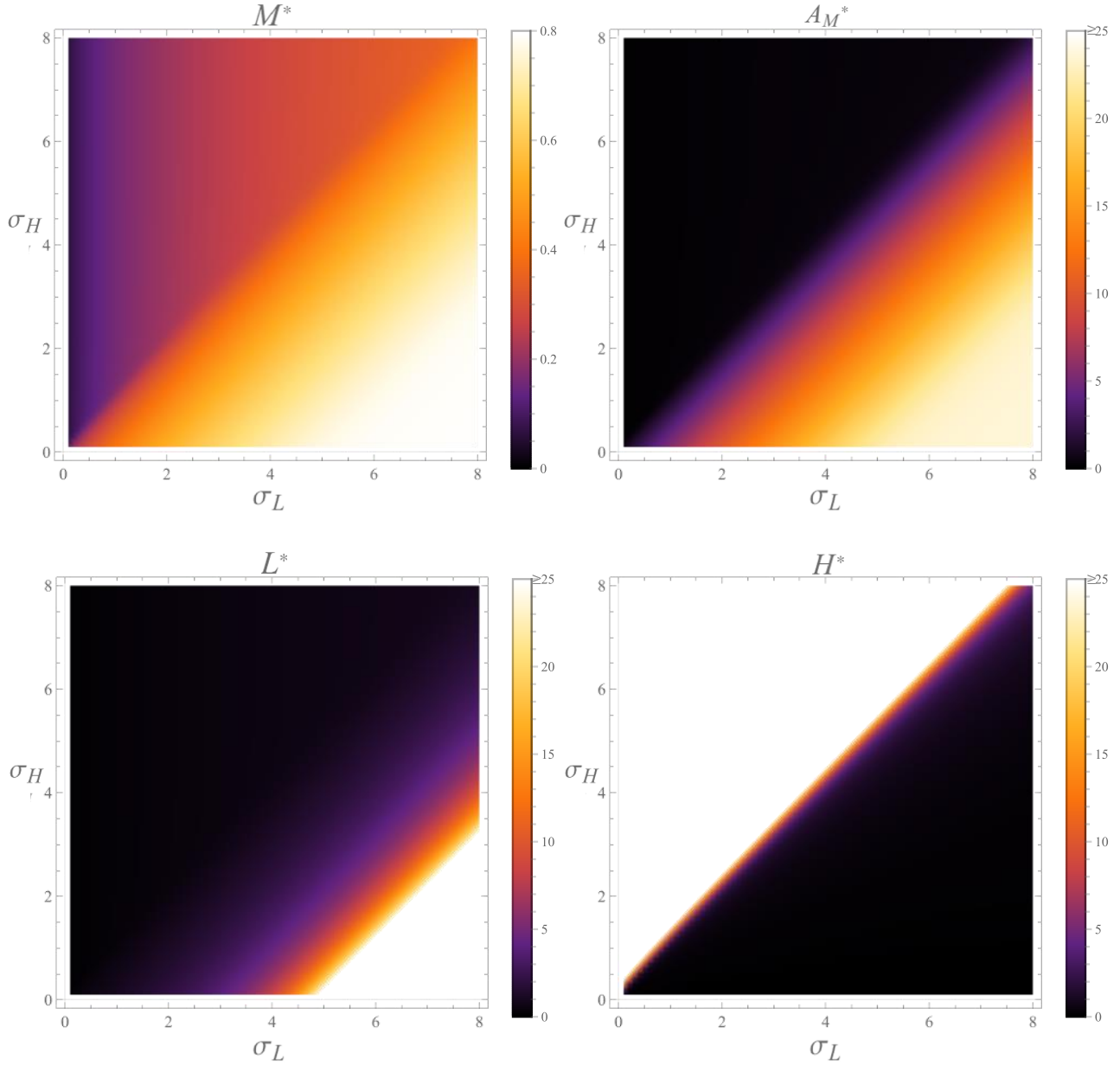


Figure 6: **Plaque composition is sensitive to the influxes of LDL ( $\sigma_L$ ) and HDL ( $\sigma_H$ ).** The steady state values  $M^*$ ,  $A_M^*$ ,  $L^*$  and  $H^*$  are plotted against  $\sigma_L$  and  $\sigma_H$ . Note that the approximately linear contours, which feature in all four plots, indicate that the dependent variables are sensitive to the difference  $\sigma_L - \sigma_H$ , indicating that plaque composition is largely determined by the relative influx of LDL lipid to HDL capacity. Parameter values are set according to equations (25).

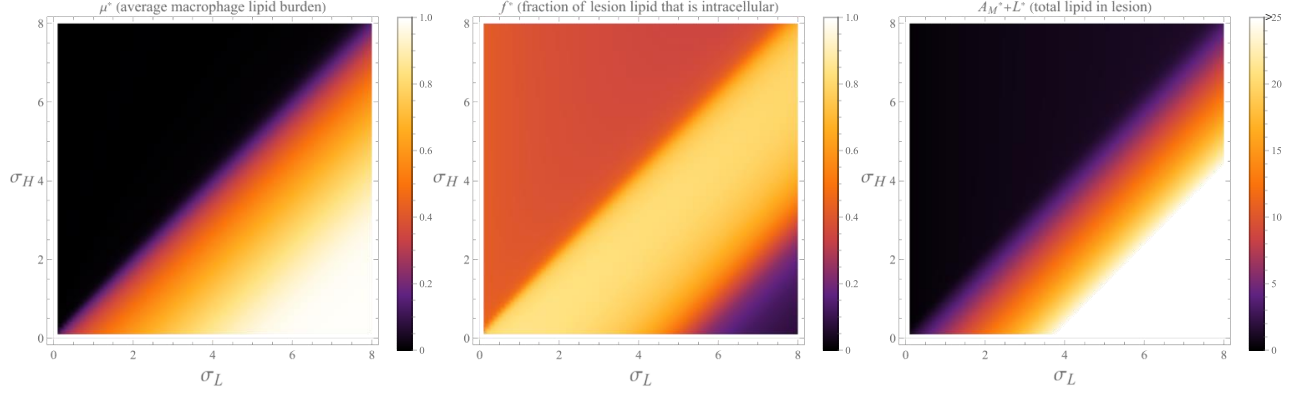


Figure 7: **Equilibrium plaque lipid content as the LDL and HDL influxes are varied.** We plot the normalised quantities  $\mu^*$  and  $f^*$ , defined by equations (26), and the total lesion lipid,  $A_M^* + L^*$  against  $\sigma_L$  and  $\sigma_H$ . Note how the fraction of lipid that is intracellular,  $f^*$ , is approximately constant in the band  $0 \lesssim \sigma_L - \sigma_H \lesssim 5$ , in which average macrophage lipid burden,  $\mu^*$ , and total lesion lipid,  $A_M^* + L^*$ , both vary substantially. The parameter values are set according to equations (25).

macrophage lipid burden),  $f^*$ , the fraction of lesion lipid that is intracellular and  $A_M^* + L^*$ , the total lesion lipid, as  $\sigma_L$  and  $\sigma_H$  vary. In contrast to the trends of  $\mu^*$  and  $A_M^* + L^*$  (which both increase with  $\sigma_L$  and decrease with  $\sigma_H$ ), the fraction  $f^*$  exhibits non-monotonic dependence on both  $\sigma_L$  and  $\sigma_H$ . It follows that  $f^*$  may be a poor metric for plaque progression since it can take the same value when plaque lipid content is low or high (e.g.  $f^* \approx 0.4$  at  $(\sigma_L, \sigma_H) = (2, 4)$  or  $(6, 2)$ ). We note further that  $f^*$  is approximately constant for  $0 \lesssim \sigma_L - \sigma_H \lesssim 5$ , while  $\mu^*$  and  $A_M^* + L^*$  vary substantially in this interval. This behaviour probably occurs because, in this region of parameter space, most of the lipid is contained in the macrophage population (compare plots for  $A_M^*$  and  $L^*$  in Fig.6), and so the primary source of extracellular lipid is cell death. Since the amount of lipid entering the extracellular environment via cell death is exactly the lipid content of the dying macrophages, cell death acts to equalise any changes in the amounts of intracellular and extracellular lipid. Finally, the plots confirm that the lesion is dominated by extracellular lipid in the region  $\sigma_L - \sigma_H \gtrsim 5$ , where macrophage lipid loads are comparable to the maximum lipid capacity.

### 3.3. Macrophage lipid distribution

It is not straightforward to analyse the lipid distribution  $m_j(t)$ ,  $j = 0, 1, \dots, J$  by directly considering equations (16)-(18). In Appendix B we show that closed-form solutions for the steady state values,  $m_j^*$ ,  $j = 0, 1, \dots, J$ , can be obtained via the method of generating functions.

The resulting steady state solutions read:

$$m_j^* = M^* \left( \prod_{\ell=1}^j \frac{a_c(J-\ell+1)}{(p+1+\ell)} \right) \sum_{n=0}^{J-j} \frac{(j+1)^{(n)}(j-J)^{(n)} a_c^n}{(j+2+p)^{(n)} n!}, \quad 0 \leq j \leq J, \quad (34)$$

where  $x^{(n)} = x(x+1)\cdots(x+n-1)$  is the  $n$ -th rising factorial of  $x \in \mathbb{R}$ , and  $a_c$  and  $p$  are the parameter groupings:

$$a_c := \frac{k_L L^*}{k_L L^* + k_H H^*}, \quad p := \frac{1 + \gamma}{k_L L^* + k_H H^*} - 1. \quad (35)$$

Although the solution (B.9) is exact, the complicated dependence of  $m_j^*$  on the index  $j$  and the model parameters makes it difficult to analyse the geometric features of the distribution (e.g. the curvature, existence of a local maximum). We show below how this information can be readily extracted from a continuum approximation of equations (16)-(18).

### 3.3.1. Derivation of continuum approximation

We identify the (dimensionless) discrete lipid distribution  $m_j(t)$ ,  $j = 0, 1, \dots, J$ , with the function  $m(a, t) \geq 0$ , which is defined over a continuous structure variable,  $a$ . Specifically, we make the identifications:

$$a \sim \frac{j}{J} \quad \text{and} \quad m(a, t) \sim J m_j(t), \quad (36)$$

so that  $0 \leq a \leq 1$  and  $m(a, t)$  is proportional to the number density of macrophages with lipid content  $a_0 + (\kappa - a_0)a$  at time  $t$ . The structure variable is bounded such that  $a = 0$  corresponds to macrophages containing only endogenous lipid and  $a = 1$  to macrophages whose lipid load is at maximum capacity. Letting  $\epsilon := J^{-1}$ , we recast the discrete equations (17) as the following non-local equation:

$$\begin{aligned} \epsilon \frac{\partial m}{\partial t}(a, t) &= k_L L [(1-a+\epsilon)m(a-\epsilon, t) - (1-a)m(a, t)] \\ &\quad + k_H H [(a+\epsilon)m(a+\epsilon, t) - am(a, t)] - (1+\gamma)m(a, t), \end{aligned} \quad (37)$$

where  $\epsilon \leq a \leq 1 - \epsilon$ . We derive our continuum model by using a Taylor series approximation to expand the terms in equation (37) about  $\epsilon = 0$  and extending the domain of validity to  $0 \leq a \leq 1$ . Dividing through by  $\epsilon$  and retaining terms of  $O(\epsilon)$  yields the PDE:

$$\frac{\partial m}{\partial t} = k_L L \left[ -\frac{\partial}{\partial a} + \frac{\epsilon}{2} \frac{\partial^2}{\partial a^2} \right] [(1-a)m] + k_H H \left[ \frac{\partial}{\partial a} + \frac{\epsilon}{2} \frac{\partial^2}{\partial a^2} \right] [am] - (1+\gamma)m. \quad (38)$$

Equation (38) is an advection-diffusion equation. In conservation form, it reads:

$$\frac{\partial m}{\partial t} = \frac{\partial}{\partial a} \left[ D(a, t) \frac{\partial m}{\partial a} - v(a, t)m \right] - (1 + \gamma)m, \quad (39)$$

where the lipid content velocity,  $v$ , and diffusion coefficient,  $D$ , are defined as follows:

$$v(a, t) := k_L L(1 - a) - k_H H a + \frac{\epsilon}{2}(k_L L - k_H H), \quad (40)$$

$$D(a, t) := \frac{\epsilon}{2}(k_L L(1 - a) + k_H H a). \quad (41)$$

Appropriate boundary conditions are determined by considering the dynamics of the dimensionless macrophage population,  $M(t)$ , which, in the continuum formulation, we identify with the integral:

$$M(t) \sim \int_0^1 m(a, t) da. \quad (42)$$

Integrating equation (39) with respect to  $a \in (0, 1)$ , we deduce that:

$$\frac{dM}{dt} = \left( D \frac{\partial m}{\partial a} - vm \right) \Big|_{a=0}^{a=1} - (1 + \gamma)M. \quad (43)$$

To ensure consistency between equations (43) and (19), we set:

$$\left( D \frac{\partial m}{\partial a} - vm \right) \Big|_{a=0} = -\frac{L}{L_c + L}, \quad \text{and} \quad \left( D \frac{\partial m}{\partial a} - vm \right) \Big|_{a=1} = 0. \quad (44)$$

The boundary condition at  $a = 0$  ensures that the flux of macrophages at  $a = 0$  is given by the macrophage recruitment rate, while the no-flux condition at  $a = 1$  ensures that macrophages cannot exceed the maximal lipid load  $a = 1$ . Finally, we impose the initial condition:

$$m(a, 0) = 0, \quad (45)$$

and close the continuum model by coupling the PDE to the ODE subsystem (19)-(21).

### 3.3.2. Comparison of discrete and continuum models

We generate numerical solutions of the continuum model, defined by equations (39),(44), (45), (19)-(23), by using the Method of Lines, with second-order central differencing for  $\frac{\partial m}{\partial a}$  and  $\frac{\partial^2 m}{\partial a^2}$ . The output is compared to that of the discrete model (16)-(23) in Figure 8. We find that the discrete and continuum models are in excellent agreement, with better consistency for smaller values of  $\epsilon$  and late time points,  $t$ . We note that the value of  $\epsilon$  appears to affect

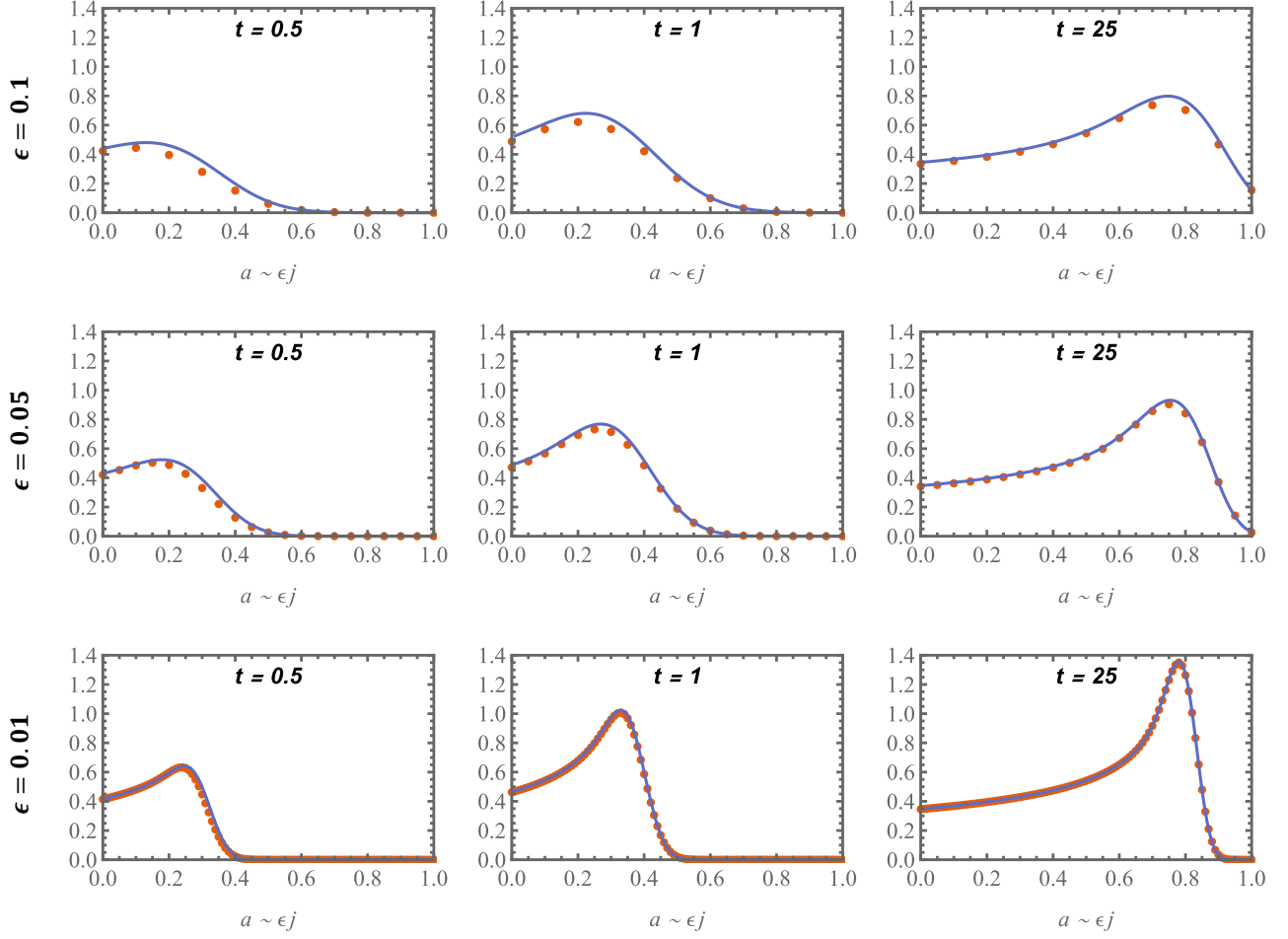


Figure 8: **Continuum vs. discrete models.** The output for the discrete model (16)-(23) is compared to that of the continuum model(39),(44), (45), (19)-(23) for  $\epsilon = 0.1, 0.05$  and  $0.01$  in the top, middle and bottom rows respectively. The distributions are shown at the times  $t = 0.5, 1$  and  $25$ , where the system is approximately at equilibrium. The other parameters are set to:  $\sigma_L = 3, k_L = 1, k_H H = 0.3, \kappa = 30, \gamma = 0.25$  and  $L_c = 1$ .

the sharpness of the wavefront, but not its location, with smaller values of  $\epsilon$  yielding sharper wavefronts. These observations are consistent with equations (40) and (41), which show that the diffusion coefficient,  $D(a, t)$ , is proportional to  $\epsilon$ , while the velocity,  $v(a, t)$ , is an  $\mathcal{O}(1)$  quantity.

We quantify the deviation between the discrete and continuum models at time  $t$  by defining the mean-squared error (MSE):

$$\text{MSE}(t; \epsilon) := \frac{1}{J} \sum_{j=0}^J (Jm_j(t) - m(j/J, t))^2, \quad (46)$$

where  $J = \epsilon^{-1}$ , and  $m_j(t)$  and  $m(\cdot, t)$  are the discrete and continuum distributions respectively. In Appendix C we plot the MSE across a number of sample times  $t$  and values of  $\epsilon$ . The good agreement between the discrete and continuum models is reflected in that  $\text{MSE} < 2 \times 10^{-3}$  for all samples. The largest deviation between the models occurs at early times  $0 < t < 1$ . This transient difference is suppressed on an  $\mathcal{O}(1)$  timescale.

### 3.4. Asymptotic analysis at steady state

Let  $m^*(a) = \lim_{t \rightarrow \infty} m(a, t)$  denote the steady lipid distribution for the continuum model. Setting the time derivative to zero in equation (39) and rearranging, we have that:

$$\frac{\epsilon}{2} [a_c - (2a_c - 1)a] \frac{d^2 m^*}{da^2} + [\epsilon(2a_c - 1) + (a - a_c)] \frac{dm^*}{da} - pm^* = 0, \quad (47)$$

where the constants  $a_c$  and  $p$  are given by:

$$a_c := \frac{k_L L^*}{k_L L^* + k_H H^*}, \quad p := \frac{1 + \gamma}{k_L L^* + k_H H^*} - 1. \quad (48)$$

Recall that  $L^* > 0$  and  $H^* > 0$  are the steady state values of  $L(t)$  and  $H(t)$  respectively. It follows that  $0 < a_c < 1$  and  $p > -1$ . In what follows, we view  $a_c$  and  $p$  as  $\mathcal{O}(1)$  quantities.

At steady state the boundary conditions (44) are:

$$\frac{\epsilon}{2} \frac{dm^*}{da} - \left[ 1 + \frac{\epsilon}{2} \left( \frac{2a_c - 1}{a_c} \right) \right] m^* = -R, \quad \text{at } a = 0, \quad (49)$$

$$\frac{\epsilon}{2} \frac{dm^*}{da} + \left[ 1 - \frac{\epsilon}{2} \left( \frac{2a_c - 1}{1 - a_c} \right) \right] m^* = 0, \quad \text{at } a = 1, \quad (50)$$

where  $R := \frac{1}{k_L(L^* + L_c)}$  is a rescaled recruitment rate. Equations (47)-(50) define a singular perturbation problem with respect to the small parameter  $\epsilon \ll 1$ . We use the method of

matched asymptotics to construct a uniformly valid approximate solution for  $m^*(a)$  in the limit  $\epsilon \rightarrow 0$ .

By setting  $\epsilon = 0$  in equations (47), (49), (50), we deduce that the leading order outer solutions satisfy:

$$(a - a_c) \frac{dm^*}{da} - pm^* = 0 \quad (51)$$

and are subject to the Dirichlet conditions:

$$m^*(0) = R, \quad m^*(1) = 0. \quad (52)$$

The general solution to equation (51) is given by:

$$m^*(a) = K \left(1 - \frac{a}{a_c}\right)^p, \quad (53)$$

where  $K$  is a constant of integration. Since we cannot enforce both boundary conditions (52) simultaneously, we deduce that there are two outer solutions:

$$m_{\text{left}}^*(a) := R \left(1 - \frac{a}{a_c}\right)^p, \quad m_{\text{right}}^*(a) := 0. \quad (54)$$

The left solution  $m_{\text{left}}^*(a)$  is well-defined for  $0 \leq a < a_c$ , while  $m_{\text{right}}^*(a)$  holds in a neighbourhood of  $a = 1$ . We form the following composite solution:

$$m_{\text{outer}}^*(a) := \begin{cases} R \left(1 - \frac{a}{a_c}\right)^p, & 0 \leq a < a_c, \\ 0, & a_c < a \leq 1, \end{cases} \quad (55)$$

which ensures continuity in  $m_{\text{outer}}^*$  at  $a = a_c$  for  $p > 0$ .

Numerical solutions of the continuum model indicate that  $m_{\text{outer}}^*(a)$  is a good approximation to  $m^*(a)$  away from the critical value  $a = a_c$  (see Figure 9). For  $p > 0$ , as in Fig.9a, the outer solution (55) is continuous at  $a = a_c$ , but the numerical solution has a smoother transition towards the zero solution as  $a$  increases. For  $p = 0$ , shown in Fig.9b, the solution (55) is piecewise constant with a discontinuity at  $a = a_c$ . By contrast, the numerical solution is continuous for all  $0 < a < 1$  and takes on a sigmoid profile. For  $p < 0$ , as in Fig.9, the solution (55) diverges as  $a \rightarrow a_c^-$ , while the numerical solution has a local maximum near  $a = a_c$  in this case.

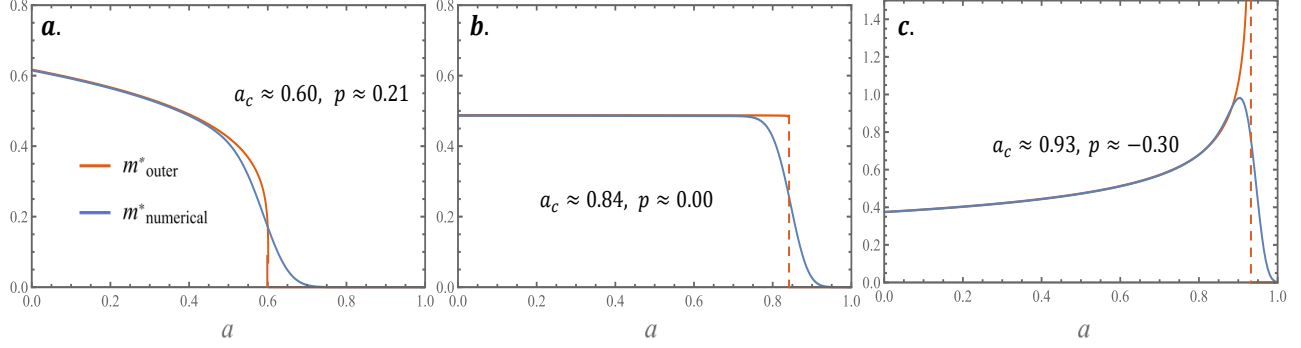


Figure 9: **Composite outer solution.** The outer solution (55) is compared with the numerical solution for  $m^*(a)$  for three values of the LDL influx,  $\sigma_L$ . The numerical solution is generated by solving the time-dependent system (39),(44), (45), (19)-(23) to  $t = 200$ . We use  $\sigma_L = 1.3, 1.845$  and  $2.5$  in cases a,b and c respectively. The red dashed line in cases b and c indicate the discontinuity of  $m^*_{\text{outer}}$  at  $a = a_c$ . We fix  $\sigma_H = 1$  and set the remaining parameters to the default values stated in equations (25).

These observations suggest that we may use  $p$  and  $a_c$  to characterise the solution  $m^*(a)$  of the full equation (47). The value of  $p$  determines the geometric features of  $m^*(a)$ . For  $p > 0$ , the solution is a decreasing function of  $a$ . The curvature is determined by whether  $p > 1$ , giving a concave-up  $m^*(a)$  for  $0 < a \lesssim a_c$ , or  $0 < p < 1$ , where  $m^*(a)$  is concave-down for  $0 < a \lesssim a_c$ . If  $p = 0$ , then  $m^*(a)$  is a sigmoid and constant away from  $a = a_c$ . Finally, if  $p < 0$ , then  $m^*(a)$  attains a local maximum near  $a = a_c$ , with the sharpness of the peak growing as  $p \rightarrow (-1)^+$ .

We show how  $p$  and  $a_c$  depend on  $\sigma_L$  and  $\sigma_H$  in Figure 10. We find that the contours of constant  $a_c$  (Fig.10a) are approximately linear in  $(\sigma_L, \sigma_H)$  space, and indicate that  $a_c$  increases sensitively with  $(\sigma_L - \sigma_H)$ . By contrast, the value of  $p$  (Fig.10b) is non-monotonic in both  $\sigma_L$  and  $\sigma_H$ , and diverges at the origin:  $p \rightarrow \infty$  as  $(\sigma_L, \sigma_H) \rightarrow (0, 0)$ . The critical contours,  $p = 0$  and  $p = 1$ , are indicated so that we may partition  $(\sigma_L, \sigma_H)$  space according to the qualitative behaviour of the steady state profile of  $m^*(a)$ . Consistent with the numerical results of Section 3.1, we find that  $m^*(a)$  has a peaked profile ( $p < 0$ ) when either  $\sigma_L$  or  $\sigma_H$  are large enough. Comparison with the corresponding value of  $a_c$  reveals that peaked profiles can occur with the local maximum at low or high lipid loads (location of peak is approximately  $a_c$ ). Furthermore,  $m^*(a)$  only adopts a decreasing and convex profile when  $\sigma_L$  and  $\sigma_H$  are both sufficiently small.

To attain a uniformly valid approximation for  $m^*(a)$  over  $0 < a < 1$ , we define an interior variable  $a = a_c + \epsilon^n \sqrt{2a_c(1 - a_c)} \tilde{a}$  where  $n > 0$  is to be specified and the coefficient of  $\tilde{a}$  is

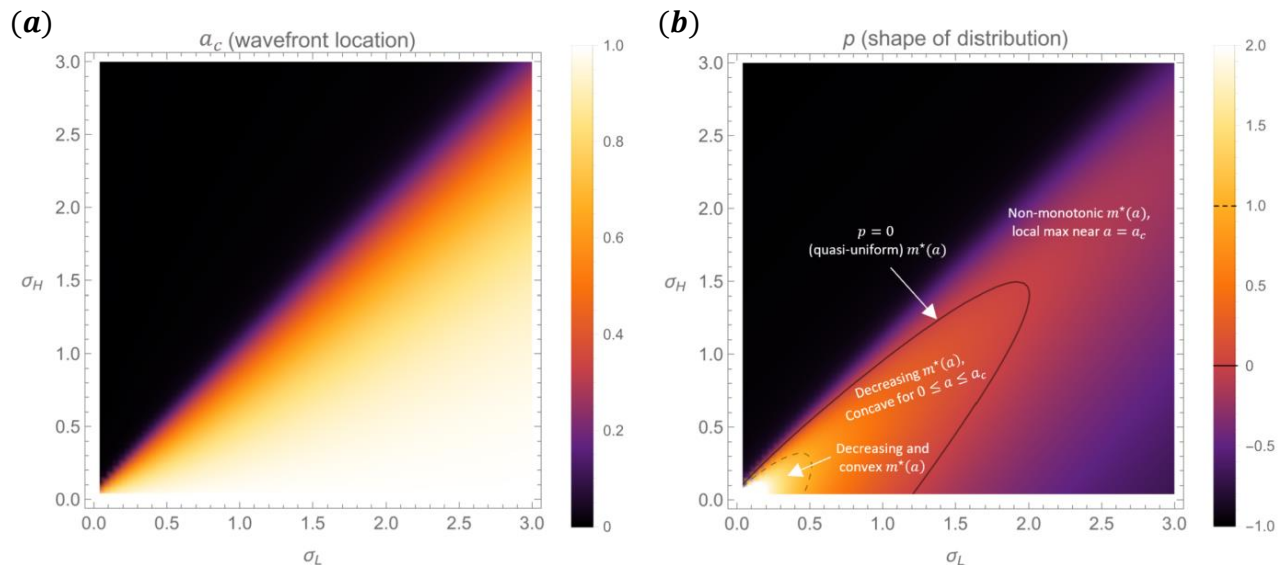


Figure 10: **Characterisation of the equilibrium macrophage lipid distribution,  $m^*(a)$ , in terms of LDL influx,  $\sigma_L$ , and HDL influx,  $\sigma_H$ .** Plot (a) shows the value of  $a_c$ , which approximates the lipid content of the most lipid-laden macrophage at equilibrium. Plot (b) indicates the value of the parameter  $p$ , which determines the shape of the distribution as indicated. Parameter values are set according to equations (25).

chosen to simplify the interior equation. Under this change of variables, equation (47) becomes:

$$\frac{\epsilon^{1-2n}}{2} \left[ 1 + \epsilon^n \frac{1 - 2a_c}{2a_c(1 - a_c)} \tilde{a} \right] \frac{d^2 m^*}{d\tilde{a}^2} + \left[ \epsilon^{1-n} \frac{2a_c - 1}{\sqrt{2a_c(1 - a_c)}} + \tilde{a} \right] \frac{dm^*}{d\tilde{a}} - pm^* = 0, \quad (56)$$

for  $-\infty < \tilde{a} < \infty$ . In order to match to the two outer solutions we choose  $n$  such that a term proportional to  $\frac{d^2 m^*}{d\tilde{a}^2}$  becomes comparable to the  $O(1)$  terms. The smallest value of  $n$  for which this occurs is  $n = \frac{1}{2}$ , which gives the following equation at leading order:

$$\frac{1}{2} \frac{d^2 m^*}{d\tilde{a}^2} + \tilde{a} \frac{dm^*}{d\tilde{a}} - pm^* = 0. \quad (57)$$

The general solution to equation (57) is:

$$m_{\text{interior}}^*(\tilde{a}) = e^{-\tilde{a}^2} \left[ K_1 H_{-1-p}(\tilde{a}) + K_2 {}_1F_1\left(\frac{1+p}{2}, \frac{1}{2}, \tilde{a}^2\right) \right], \quad (58)$$

where  $H$  and  ${}_1F_1$  are the Hermite and Kummer confluent hypergeometric functions respectively ([29, 30]). The constants of integration,  $K_1$  and  $K_2$ , are determined by matching  $m_{\text{interior}}^*$  to the outer solutions  $m_{\text{left}}^*$  and  $m_{\text{right}}^*$  respectively. We note that equation (58) satisfies the following

asymptotic relation as  $\tilde{a} \rightarrow \infty$ :

$$\begin{aligned} m_{\text{interior}}^* &\sim K_2 \frac{\pi^{1/2}}{\Gamma((1+p)/2)} \tilde{a}^p \\ &= K_2 \frac{\pi^{1/2}}{\Gamma((1+p)/2)} \epsilon^{-p/2} (a - a_c)^p. \end{aligned} \quad (59)$$

Comparing with  $m_{\text{right}}^*(a)$  shows that we must take  $K_2 = 0$ . As  $\tilde{a} \rightarrow -\infty$ , we use that:

$$\begin{aligned} m_{\text{interior}}^* &\sim -K_1 \pi^{1/2} \Gamma(-p) \sin(p\pi) (-\tilde{a})^p \\ &= -K_1 \pi^{1/2} \Gamma(-p) \sin(p\pi) a_c^p \epsilon^{-p/2} \left(1 - \frac{a}{a_c}\right)^p, \end{aligned} \quad (60)$$

and compare with  $m_{\text{left}}^*(a)$  to deduce that the matched interior solution is:

$$m_{\text{interior}}^*(\tilde{a}) = K_1 e^{-\tilde{a}^2} H_{-1-p}(\tilde{a}), \quad \text{where} \quad K_1 = \frac{-R\sqrt{\pi}[2\epsilon a_c(1-a_c)]^{p/2}}{a_c^p \Gamma(-p) \sin(p\pi)}. \quad (61)$$

We note that  $\Gamma(-p) \sin(p\pi) < 0$  for all  $p > -1$  and so  $K_1 > 0$ .

The function  $m_{\text{interior}}^*/K_1$  from (61) is plotted for various values of  $p$  in Figure 11. We divide by  $K_1$  since it affects only the vertical scale of the interior solution. The function becomes increasingly asymmetric as  $p$  increases, transitioning from a bell curve at  $p = -1$ , to a sigmoid at  $p = 0$ , and eventually a smoothed corner-like shape for  $p > 0$ . Consistent with these observations, we find that  $m_{\text{interior}}^*$  reduces exactly to a Gaussian in the limit  $p \rightarrow (-1)^+$  and a sigmoid at  $p = 0$ :

$$m_{\text{interior}}^*(\tilde{a}) \rightarrow K_1 e^{-\tilde{a}^2}, \quad p \rightarrow (-1)^+; \quad (62)$$

$$m_{\text{interior}}^*(\tilde{a}) = \frac{K_1 \sqrt{\pi}}{2} \text{erf}(\tilde{a}), \quad p = 0. \quad (63)$$

A leading order approximation for  $m^*(a)$  that is uniformly valid over  $0 \leq a \leq 1$  is obtained by substituting  $\tilde{a} = [2\epsilon a_c(1-a_c)]^{-1/2}(a-a_c)$  into equation (61):

$$m_{\text{asymptotic}}^*(a) = K_1 \exp \left[ -\frac{(a-a_c)^2}{2\epsilon a_c(1-a_c)} \right] H_{-1-p} \left( \frac{a-a_c}{\sqrt{2\epsilon a_c(1-a_c)}} \right). \quad (64)$$

We compare the matched solution (64) to the discrete model output in Figure 12. The plots show an excellent agreement between the asymptotic solution and discrete model.

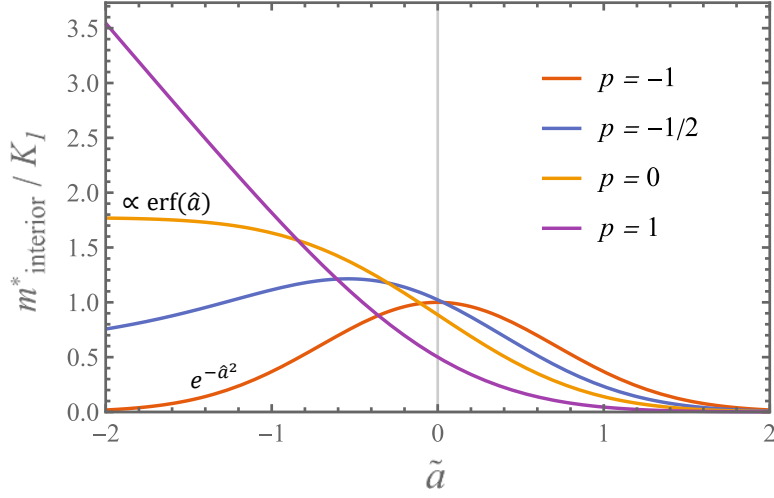


Figure 11: **The interior solution.** The function  $e^{-\tilde{a}^2} H_{-1-p}(\tilde{a})$  from the interior solution (61) is shown for the values  $p = -1$  (limiting case, Gaussian),  $-1/2$ ,  $0$  (sigmoid) and  $1$ .

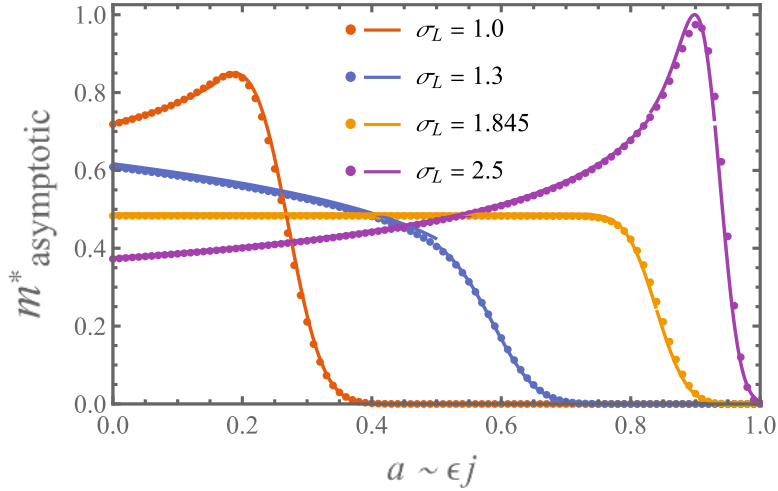


Figure 12: **Asymptotic solution vs discrete model output.** The asymptotic solution of the continuum model, defined by equation (64), is plotted with the discrete model steady state distribution,  $Jm_j^*$ . We use  $\sigma_H = 1$  and set the remaining parameter values according to equations (25).

## 4. Discussion

In this paper we presented a discretely structured population model for lipid accumulation in atherosclerotic plaque macrophages. The model is formulated in terms of the amount of extracellular lipid,  $L(t)$ , the lipid capacity of the HDL particles,  $H(t)$ , and the macrophage population,  $m_j(t)$ , which is structured by an index,  $j$ , according to lipid content. A key feature of the model is that lipid uptake and offloading events cause a finite change,  $\Delta a$ , to macrophage lipid content. Our discretely-structured model formulation contrasts to the continuum approach proposed by Ford et al. [17]. It can also be reduced to a simpler subsystem of ODEs for  $L(t)$ ,  $H(t)$ , the total number of macrophages,  $M(t)$ , and the total macrophage lipid content,  $A_M(t)$ .

A defining feature of our model is the treatment of macrophage lipid uptake and offloading: the uptake rate is assumed to decrease linearly with lipid content,  $k_L(1 - j/J)$ , while the offloading rate increases linearly, according to  $k_H j/J$ . These assumptions are consistent with current understanding that macrophages have a finite capacity for phagocytosis due to intracellular negative-feedback signalling [7], and that intracellular cholesterol accumulation promotes the up-regulation of transporters that mediate cholesterol efflux [8]. An important consequence of our model formulation is that macrophages have a maximal lipid content,  $j \leq J$ , since the uptake rate decreases to zero at  $j = J$ . By contrast, the model proposed by Ford et al. [17]) assumes that lipid uptake and offloading are independent of lipid content, and that there is no upper bound on macrophage lipid content. We further note that our simplifying assumption of linear dependence in  $j$  for the uptake and offloading rates ensures the existence of a closed ODE subsystem: (21)-(23). If the lipid-dependent rates were nonlinear in  $j$ , the dynamics of  $A_M(t)$  would not be expressible in terms of  $M(t)$ ,  $A_M(t)$ ,  $L(t)$  and  $H(t)$ , and opportunities for mathematical analysis would be limited.

Our model analysis focused on the constants  $\sigma_L$  and  $\sigma_H$  which determine the influx of LDL lipid and HDL capacity respectively. These parameters are expected to correlate strongly with blood LDL and HDL particle concentrations. We used the ODE subsystem to determine how changing the values of  $\sigma_L$  and  $\sigma_H$  impacts overall plaque composition and macrophage lipid distribution.

Numerical solutions showed that, at long times, the plaque develops to a nonzero equilibrium. The dynamics proceed through various stages that are detailed in Section 3.1. Consider-

ing firstly the ODE subsystem, we note that  $M(t)$  increases with  $t$ , but  $A_M(t)$ ,  $L(t)$  and  $H(t)$  may be non-monotonic; the plaque has a steadily increasing population of macrophages, but the dynamics of its intracellular lipid, extracellular lipid and unloaded HDL content may not be monotonic. Further, the subsystem dynamics are sensitive to  $(\sigma_L - \sigma_H)$ , the influx of LDL lipid relative to HDL capacity. As expected, the higher the entry rate of LDL lipid to HDL capacity, the higher the lipid accumulation in the plaque. The macrophage lipid distribution  $m_j(t)$  evolves in a wave-like manner towards its steady state solution. The wavefront velocity changes over time and may change sign (i.e., the front travels back to lower lipid loads) if  $H(t)$  is sufficiently large; average macrophage lipid loads may decrease when offloading to HDL exceeds phagocytosis. We note that the equilibrium lipid distribution,  $m_j$ , takes one of several qualitatively distinct shapes. These profiles may be monotone decreasing (concave or convex), quasi-uniform and or uni-modal. The equilibrium profile is sensitive to the individual values of  $\sigma_L$  and  $\sigma_H$ , rather than their difference,  $(\sigma_L - \sigma_H)$ .

Steady state analysis of the subsystem (19)-(22) shows that the model has a unique physically-realistic equilibrium. Analysis of the steady state solutions (see Figure 6) indicated that the number of macrophages,  $M^*$ , amounts of intracellular lipid,  $A_M^*$ , extracellular lipid,  $L^*$ , and HDL capacity,  $H^*$ , depend sensitively on the difference  $(\sigma_L - \sigma_H)$ . Hence, the model predicts that plaque composition is strongly dependent on the difference between the influx of LDL lipid relative to HDL capacity. More specifically, the plots suggest that  $(\sigma_L, \sigma_H)$  space can be partitioned into three regions. Regions in which  $\sigma_L - \sigma_H \lesssim 0$  correspond to healthy tissues in which the HDL capacity greatly exceeds the amounts of ingested and extracellular lipid. Where  $0 \lesssim \sigma_L - \sigma_H \lesssim 5$ , the HDL capacity is typically exhausted and plaques contain intermediate quantities of macrophages and lipid. Finally, regions in which  $\sigma_L - \sigma_H \gtrsim 5$  correspond to unhealthy plaques that are dominated by extracellular lipid and macrophages with lipid loads near capacity.

Equations (16)-(18) for the dynamics of  $m_j(t)$ ,  $j = 0, 1, \dots, J$ , are difficult to analyse directly. Nonetheless, we show in Appendix B that an exact solution (B.9) for the equilibrium values,  $m_j^*$ , can be constructed via the method of generating functions. Unfortunately, the solution is too complicated to extract any biological insight. Instead, we analysed the macrophage lipid distribution by deriving a continuum analogue of the discrete model. The continuum

model casts the macrophage population as a single function,  $m(a, t)$ , where the continuous independent variable  $0 \leq a \leq 1$  represents lipid content. The distribution  $m(a, t)$  is governed by an advection-diffusion PDE (39) with appropriate boundary conditions (44).

We used the method of matched asymptotics to construct a leading order approximation to the equilibrium macrophage lipid distribution,  $m^*(a)$ , in the limit  $\epsilon = J^{-1} \rightarrow 0$ . We found that  $m^*(a)$  depends on two parameter groupings:  $0 < a_c < 1$  and  $p > -1$ , defined in (48). The constant  $a_c$  approximates the maximal lipid load attained by an individual macrophage at equilibrium, and represents the macrophage lipid load where uptake balances offloading. Near  $a = a_c$ , the advection velocity is  $\mathcal{O}(\epsilon)$ , and comparable to the diffusion terms. The quantity  $p$  determines the shape of  $m^*(a)$ . Using the outer solution (55) as a guide, we found that  $m^*(a)$  is decreasing and convex for  $p > 1$ , decreasing and concave for  $0 < a \lesssim a_c$  when  $0 < p < 1$ , quasi-uniform for  $p = 0$ , and unimodal with a local maximum near  $a = a_c$  for  $p < 0$ . We note that the outer solution is discontinuous at  $a = a_c$  for  $p \leq 0$ , and in the first derivative for  $0 < p < 1$  (see Figure 9). Analysis within an interior region of  $O(\epsilon^{1/2})$  width at  $a = a_c$  is needed to construct a uniformly valid approximation for  $m^*(a)$ , resulting in the solution (64). These observations highlight the importance of including second-order terms in the continuum approximation to capture the qualitative behaviour of the underlying discrete model. The second-order terms provide a diffusive effect that smooths the outer solution in the interior region where the advection velocity vanishes at first order.

Figure 10 shows that the parameter groupings  $a_c$  and  $p$  are sensitive to the influxes of LDL lipid ( $\sigma_L$ ) and HDL capacity ( $\sigma_H$ ). Like the steady state values of the reduced subsystem variables, the constant  $a_c$  increases with  $(\sigma_L - \sigma_H)$ ; the higher the influx of LDL lipid relative to HDL capacity, the higher the lipid load of the most lipid-laden macrophage in the population. In particular, by comparing Figures 7 and 10 we see that  $a_c$  and  $\mu^*$  (average macrophage lipid burden, or equivalently the fractional defect in phagocytosis due to lipid loading) are highly correlated. Noting that  $a_c \gtrsim 0.99$  and  $\mu^* \gtrsim 60\%$  for  $\sigma_L - \sigma_H \gtrsim 3$ , the model indicates that plaque macrophages can expect at least a 60% decrease in their population-averaged phagocytosis rate (purely due to lipid accumulation) if macrophages with lipid content near the capacity value,  $a = 1$ , are detected. These results show that the phagocytic efficiency of macrophage populations *in vivo* may be markedly reduced by intracellular lipid accumulation. In particular,

intracellular lipid accumulation may serve as a partial explanation for the defective efferocytosis often observed in atherosclerotic plaques [11, 31]. The model also indicates that this hypothesis may be verified experimentally if macrophages with lipid content near capacity are detected *in vivo*.

By contrast, the parameter  $p$  is non-monotonic in both  $\sigma_L$  and  $\sigma_H$ , and, hence, the shape of the distribution  $m^*(a)$  depends on the individual influxes of LDL lipid and HDL capacity. In particular,  $m^*(a)$  may adopt a peaked or quasi-uniform profile at low or high lipid loads. These results suggest that, unlike the maximally attained lipid load  $a_c$ , the geometric features of the macrophage lipid distribution, such as the concavity and existence of local maximum, may be poor indicators of plaque progression.

There are many ways in which our model could be extended. For instance the model assumes that the rates of macrophage death and emigration are constant. However, experimental observations indicate that lipid acquisition can induce cytotoxic macrophage death [32], and lipid-laden macrophages are less capable of emigration [33]. These effects could be accommodated by viewing  $\beta$  as an increasing function of  $j$  and  $\gamma$  as a decreasing function of  $j$ . Lipid-dependent death and emigration rates are the focus of a study by Watson et al. ([19]). Based upon their results, we expect lipid-dependent death and emigration rates to increase the overall plaque lipid burden relative to the prediction of our model, with more macrophages bearing high lipid loads. Our model further assumes that macrophage proliferation is negligible. However, experiments show that, although proliferation is more significant in the later stages of plaque development, it is still detectable in early plaques (Robbins et al. [34]). The effect of proliferation on lipid accumulation in atherosclerosis is the focus of the model by Chambers et al. ([18]). Based upon their results, we anticipate that incorporating proliferation into our model will decrease the average lipid burden of the macrophages, opposing the effects of lipid-dependent cell death and emigration.

We could also extend the model to account for spatial variation in the dependent variables. This would allow us to study the spatial distribution of intracellular lipid, and to determine how the location and shape of the extracellular lipid core change as model parameters vary. Such an extended model would be similar in form to the spatially resolved phenotype-structured models of tumour growth by Celora et al. [35] and Fiandaca et al. [36]. Based on these works,

we anticipate that analysis of a spatially explicit lipid-structured model would rely primarily on numerical simulations.

The current model further assumes that the rate of macrophage recruitment increases with the amount of extracellular lipid,  $L(t)$ . A more realistic treatment of recruitment would account for the production of pro-inflammatory and anti-inflammatory/pro-mediating signals by macrophages, which ultimately requires a treatment of macrophage phenotype. One possibility, explored in Ford et al. [17], is to assume recruitment increases with macrophage lipid burden. However, this assumption is at odds with experimental studies that indicate lipid-laden macrophages express fewer inflammatory genes compared with macrophages with a lesser lipid burden [37]. Another approach, which we will pursue in a future study, is to treat phenotype as a separate structure variable that determines the recruitment rate, and distinguish between pro-inflammatory (e.g. uptake of modified LDL) and anti-inflammatory (e.g. efferocytosis) phagocytosis events. The inclusion of anti-inflammatory effects that dampen macrophage recruitment is likely to complicate the time-dependent behaviour of the macrophage population,  $M(t)$ , relative to the monotone increase with  $t$  observed in our model.

## 5. Conclusions

In this paper we have presented a new lipid-structured model for atherosclerotic plaque macrophages. We showed that the overall plaque composition and the distribution of lipid within the macrophage population are highly sensitive to the influxes of LDL lipid ( $\sigma_L$ ) and HDL capacity ( $\sigma_H$ ). Our results support the notion that plaque lipid content is best reduced by simultaneously lowering the bloodstream concentration of LDL and raising that of HDL. We show further how the qualitative profile of the equilibrium macrophage lipid distribution changes as  $\sigma_L$  and  $\sigma_H$  vary. These profiles may be monotone decreasing (concave or convex), quasi-uniform or unimodal. Our results also highlight that, since macrophages have a finite capacity, the efficiency of lipid uptake by macrophages may be severely impaired by lipid accumulation. Lipid accumulation in plaque macrophages may therefore serve as a partial explanation for the defective efferocytosis often observed in atherosclerotic plaques, especially if macrophages with lipid content near capacity are observed *in vivo*.

## **Declaration of competing interest**

The authors declare that they have no known competing financial interests or personal relationships that could have appeared to influence the work reported in this paper.

## **Acknowledgements**

The authors wish to thank Michael G Watson, Laura Chaffey, Gareth Purvis and David R Greaves for helpful conversations that contributed to the ideas in this article. KC acknowledges support from the Oxford Australia Scholarships Fund and Clarendon Scholars' Association.

## Appendix A. Complete statement of polynomial (29) for $L^*$

Setting the time derivatives to zero in equations (19)-(22) reveals that  $L^*$  satisfies a quintic polynomial:

$$c_5(L^*)^5 + c_4(L^*)^4 + c_3(L^*)^3 + c_2(L^*)^2 + c_1L^* + c_0 = 0, \quad (\text{A.1})$$

with the following coefficients:

$$c_0 := (\gamma + 1)^2 L_c^2 \sigma_L (\gamma \delta_H + \delta_H + k_H (\sigma_H - (\gamma + 1) \sigma_L)), \quad (\text{A.2})$$

$$\begin{aligned} c_1 := & (\gamma + 1) L_c \left[ (\gamma + 1) (\gamma + 2) L_c \delta_H k_L \sigma_L \right. \\ & + L_c k_H \left( k_L \sigma_L (\sigma_H - \sigma_L) - \sigma_H \delta_L + 2(\gamma + 1) \delta_L \sigma_L \right) - (\gamma + 1) L_c \delta_H \delta_L + \delta_H \\ & \left. - 2k_H \sigma_L (-\sigma_H + \gamma \sigma_L + \sigma_L + 1) + 2(\gamma + 1) \delta_H \sigma_L + k_H \sigma_H \right], \end{aligned} \quad (\text{A.3})$$

$$\begin{aligned} c_2 := & (\gamma + 1) (k_H (-L_c \sigma_H k_L ((\gamma + 1) L_c \delta_L + \kappa - 2) \\ & + L_c k_L \sigma_L (2\gamma (L_c \delta_L + \sigma_H + \kappa - 1) + 2L_c \delta_L + 2\sigma_H + \kappa - 3) - 2(\gamma + 1) L_c \sigma_H \delta_L \\ & + (\gamma + 1) \sigma_L (4(\gamma + 1) L_c \delta_L + \sigma_H - 2) - (\gamma + 1) \sigma_L^2 (2L_c k_L + \gamma + 1) \\ & - ((\gamma + 1) L_c \delta_L - 1)^2 + \sigma_H) + L_c \delta_H (-(\gamma + 1) \delta_L ((\gamma + 2) L_c k_L + 2(\gamma + 1)) - \gamma \kappa k_L) \\ & + (\gamma + 1) \delta_H \sigma_L (L_c k_L (L_c k_L + 2\gamma + 4) + \gamma + 1) + (\gamma + 1) \delta_H (2L_c k_L + 1)), \end{aligned} \quad (\text{A.4})$$

$$\begin{aligned} c_3 := & (\gamma + 1) \delta_H (-(\gamma + 1) (\delta_L (L_c k_L (L_c k_L + 2\gamma + 4) + \gamma + 1) \\ & - k_L (L_c k_L + 2)) - \gamma \kappa k_L (L_c k_L + 1) + (\gamma + 1) k_L \sigma_L (2L_c k_L + \gamma + 2)) \\ & + k_H (k_L ((\gamma + 1) \sigma_L (\gamma (4L_c \delta_L + \sigma_H + 2\kappa - 2) + 4L_c \delta_L + \sigma_H + \kappa - 3) \\ & - (\gamma + 1) \sigma_H (2(\gamma + 1) L_c \delta_L + \kappa - 2) - ((\gamma + 1) L_c \delta_L - 1) (2\gamma \kappa + (\gamma + 1) (L_c \delta_L - 2) + \kappa) \\ & - (\gamma + 1)^2 \sigma_L^2) - (\gamma + 1) (\kappa - 1) L_c k_L^2 (\sigma_H - \sigma_L) + (\gamma + 1)^2 (-\delta_L) (2(\gamma + 1) L_c \delta_L \\ & + \sigma_H - 2(\gamma + 1) \sigma_L - 2)), \end{aligned} \quad (\text{A.5})$$

$$\begin{aligned} c_4 := & (\gamma + 1) \delta_H k_L (k_L (\gamma (-2L_c \delta_L - \kappa + \sigma_L + 1) - 2L_c \delta_L + \sigma_L + 1) - (\gamma + 1) (\gamma + 2) \delta_L) \\ & - k_H ((\gamma + 1) k_L \delta_L (\gamma (2L_c \delta_L + \sigma_H + 2\kappa - 2\sigma_L - 2) + 2L_c \delta_L + \sigma_H + \kappa - 2\sigma_L - 3) \\ & + (\kappa - 1) k_L^2 (\gamma (L_c \delta_L + \sigma_H + \kappa - \sigma_L - 1) + L_c \delta_L + \sigma_H - \sigma_L - 1) + (\gamma + 1)^3 \delta_L^2), \end{aligned} \quad (\text{A.6})$$

$$c_5 := -[(\gamma + 1) k_L \delta_L ((\gamma + 1) \delta_H k_L + (\gamma + 1) k_H \delta_L + (\kappa - 1) k_H k_L)] \quad (\text{A.7})$$

We note that  $c_5 = \mathcal{O}(\delta_L, \delta_H)$  so that equation (A.1) is a singular perturbation problem in the limit  $\delta_L \sim \delta_H \ll 1$ .

## Appendix B. Deriving closed-form solutions for $m_j^*$

We derive the formulae (B.9) by using the method of generating functions. We set:

$$f(z, t) := \sum_{j=0}^J m_j(t) z^j, \quad 0 \leq z \leq 1. \quad (\text{B.1})$$

By differentiating equation (B.1) with respect to  $t$  and substituting the ODEs (16)-(18), we find that  $f(z, t)$  satisfies the following PDE:

$$\frac{\partial f}{\partial t} + (1-z) \left[ k_L L^* \left( Jf - z \frac{\partial f}{\partial z} \right) - k_H H^* \frac{\partial f}{\partial z} \right] = 1 - (1+\gamma)f. \quad (\text{B.2})$$

Equation (B.2) is subject to the boundary condition:

$$f(1, t) = M(t). \quad (\text{B.3})$$

At steady state equations (B.2) and (B.3) reduce to the following non-autonomous ODE initial value problem:

$$(1-z) \left[ k_L L^* \left( Jf - z \frac{df}{dz} \right) - k_H H^* \frac{df}{dz} \right] = 1 - (1+\gamma)f. \quad (\text{B.4})$$

$$f(1) = M, \quad (\text{B.5})$$

which can be solved in terms of the hypergeometric function  ${}_2F_1$ :

$$f(z) = M^* {}_2F_1 \left( 1, -J, p+2, a_c(1-z) \right), \quad (\text{B.6})$$

where  $a_c$  and  $p$  are the following parameter groupings:

$$a_c := \frac{k_L L^*}{k_L L^* + k_H H^*}, \quad p := \frac{1+\gamma}{k_L L^* + k_H H^*} - 1. \quad (\text{B.7})$$

Series expansion of the solution (B.6) about  $z = 0$  gives:

$$f(z) = M^* \sum_{j=0}^J \left( \prod_{\ell=1}^j \frac{a_c(J-\ell+1)}{(p+1+\ell)} \right) {}_2F_1(j+1, j-J, 2+j+p, a_c) z^j, \quad (\text{B.8})$$

where the summation is finite because each contribution for  $j > J$  is zero. Upon comparison with definition (B.1), we obtain:

$$\begin{aligned} m_j^* &= M^* \left( \prod_{\ell=1}^j \frac{a_c(J-\ell+1)}{(p+1+\ell)} \right) {}_2F_1(j+1, j-J, 2+j+p, a_c), \\ &= M^* \left( \prod_{\ell=1}^j \frac{a_c(J-\ell+1)}{(p+1+\ell)} \right) \sum_{n=0}^{J-j} \frac{(j+1)^{(n)} (j-J)^{(n)} a_c^n}{(j+2+p)^{(n)} n!}, \quad 0 \leq j \leq J, \end{aligned} \quad (\text{B.9})$$

where  $x^{(n)} = x(x+1)\cdots(x+n-1)$  is the  $n$ -th rising factorial of  $x$ .

## Appendix C. Deviation between discrete and continuum models

We quantify the deviation between the discrete and continuum models using the mean squared error (MSE), defined in equation (46). In Figure C.13, we plot the MSE for various values of  $\epsilon$  and times  $t$ .

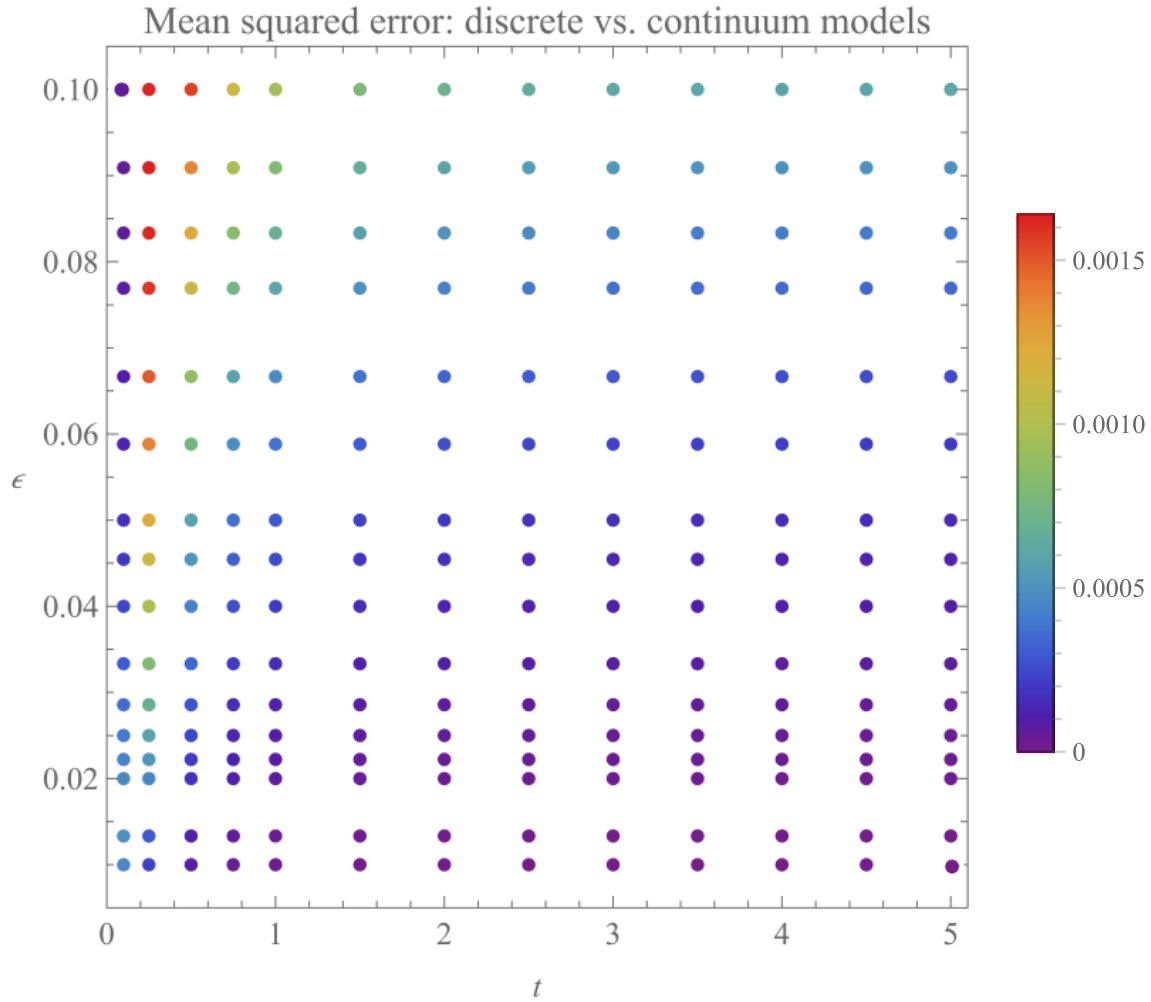


Figure C.13: **Deviation between the discrete and continuum models.** We use equation (46) to calculate the mean squared error (MSE) across a number of sample times  $t$  and values of  $\epsilon$ . The value of the MSE is indicated by the colour of the corresponding sample point. We use:  $\sigma_L = 3$ ,  $k_L = 1$ ,  $k_H H = 0.3$ ,  $\kappa = 30$ ,  $\gamma = 0.25$  and  $L_c = 1$ .

## References

- [1] M. Bäck, A. Yurdagul, I. Tabas, K. Öörni, P. T. Kovanen, Inflammation and its resolution in atherosclerosis: mediators and therapeutic opportunities, *Nature Reviews Cardiology* 16 (7) (2019) 389–406. doi:10.1038/s41569-019-0169-2.
- [2] I. Tabas, K. E. Bornfeldt, Macrophage phenotype and function in different stages of atherosclerosis, *Circulation research* 118 (4) (2016) 653–667. doi:10.1161/CIRCRESAHA.115.306256.
- [3] J. Boren, M. J. Chapman, R. M. Krauss, C. J. Packard, J. F. Bentzon, C. J. Binder, M. J. Daemen, L. L. Demer, R. A. Hegele, S. J. Nicholls, et al., Low-density lipoproteins cause atherosclerotic cardiovascular disease: pathophysiological, genetic, and therapeutic insights: a consensus statement from the european atherosclerosis society consensus panel, *European heart journal* 41 (24) (2020) 2313–2330. doi:10.1093/eurheartj/ehz962.
- [4] I. Razeghian-Jahromi, A. Karimi Akhormeh, M. Razmkhah, M. J. Zibaenezhad, Immune system and atherosclerosis: Hostile or friendly relationship, *International Journal of Immunopathology and Pharmacology* 36 (2022) 03946320221092188. doi:10.1177/03946320221092188.
- [5] J. R. Guyton, K. F. Klemp, Development of the lipid-rich core in human atherosclerosis, *Arteriosclerosis, thrombosis, and vascular biology* 16 (1) (1996) 4–11. doi:10.1161/01.ATV.16.1.4.
- [6] M. Alique, C. Luna, J. Carracedo, R. Ramírez, Ldl biochemical modifications: a link between atherosclerosis and aging, *Food & nutrition research* 59 (1) (2015) 29240. doi:10.3402/fnr.v59.29240.
- [7] C. S. Zent, M. R. Elliott, Maxed out macs: physiologic cell clearance as a function of macrophage phagocytic capacity, *The FEBS journal* 284 (7) (2017) 1021–1039. doi:10.1111/febs.13961.
- [8] A. Remmerie, C. L. Scott, Macrophages and lipid metabolism, *Cellular immunology* 330 (2018) 27–42. doi:10.1016/j.cellimm.2018.01.020.

- [9] J. J. Pinney, F. Rivera-Escalera, C. C. Chu, H. E. Whitehead, K. R. VanDerMeid, A. M. Nelson, M. C. Barbeau, C. S. Zent, M. R. Elliott, Macrophage hypophagia as a mechanism of innate immune exhaustion in mab-induced cell clearance, *Blood* 136 (18) (2020) 2065–2079. doi:10.1182/blood.2020005571.
- [10] Y. Kojima, I. L. Weissman, N. J. Leeper, The role of efferocytosis in atherosclerosis, *Circulation* 135 (5) (2017) 476–489. doi:10.1161/CIRCULATIONAHA.116.025684.
- [11] A. Yurdagul Jr, A. C. Doran, B. Cai, G. Fredman, I. A. Tabas, Mechanisms and consequences of defective efferocytosis in atherosclerosis, *Frontiers in cardiovascular medicine* 4 (2018) 86. doi:10.3389/fcvm.2017.00086.
- [12] N. A. Avgerinos, P. Neofytou, Mathematical modelling and simulation of atherosclerosis formation and progress: a review, *Annals of Biomedical Engineering* 47 (8) (2019) 1764–1785. doi:10.1007/s10439-019-02268-3.
- [13] N. El Khatib, O. Kafi, A. Sequeira, S. Simakov, Y. Vassilevski, V. Volpert, Mathematical modelling of atherosclerosis, *Mathematical modelling of natural phenomena* 14 (6) (2019) 603. doi:10.1051/mmnp/2019050.
- [14] V. Calvez, A. Ebde, N. Meunier, A. Raoult, Mathematical modelling of the atherosclerotic plaque formation, in: *Esaim: Proceedings*, Vol. 28, EDP Sciences, 2009, pp. 1–12. doi:10.1051/proc/2009036.
- [15] A. D. Chalmers, C. A. Bursill, M. R. Myerscough, Nonlinear dynamics of early atherosclerotic plaque formation may determine the efficacy of high density lipoproteins (hdl) in plaque regression, *PLoS One* 12 (11) (2017) e0187674. doi:10.1371/journal.pone.0187674.
- [16] T. Silva, W. Jäger, M. Neuss-Radu, A. Sequeira, Modeling of the early stage of atherosclerosis with emphasis on the regulation of the endothelial permeability, *Journal of Theoretical Biology* 496 (2020) 110229. doi:10.1016/j.jtbi.2020.110229.
- [17] H. Z. Ford, H. M. Byrne, M. R. Myerscough, A lipid-structured model for macrophage populations in atherosclerotic plaques, *Journal of Theoretical Biology* 479 (2019) 48–63. doi:10.1016/j.jtbi.2019.07.003.

- [18] K. L. Chambers, M. G. Watson, M. R. Myerscough, A lipid-structured mathematical model of atherosclerosis with macrophage proliferation, arXiv preprint arXiv:2205.04715 (2022). doi:10.48550/arXiv.2205.04715.
- [19] M. G. Watson, K. L. Chambers, M. R. Myerscough, A lipid-structured model of atherosclerotic plaque macrophages with lipid-dependent kinetics, arXiv preprint arXiv:2205.05285 (2022). doi:10.48550/arXiv.2205.05285.
- [20] N. Meunier, N. Muller, Mathematical study of an inflammatory model for atherosclerosis: a nonlinear renewal equation, *Acta Applicandae Mathematicae* 161 (1) (2019) 107–126. doi:10.1007/s10440-018-0206-x.
- [21] J. W. Williams, K. Zaitsev, K.-W. Kim, S. Ivanov, B. T. Saunders, P. R. Schrank, K. Kim, A. Elvington, S. H. Kim, C. G. Tucker, et al., Limited proliferation capacity of aortic intima resident macrophages requires monocyte recruitment for atherosclerotic plaque progression, *Nature immunology* 21 (10) (2020) 1194–1204. doi:10.1038/s41590-020-0768-4.
- [22] H. Z. Ford, L. Zeboudj, G. S. Purvis, A. Ten Bokum, A. E. Zarebski, J. A. Bull, H. M. Byrne, M. R. Myerscough, D. R. Greaves, Efferocytosis perpetuates substance accumulation inside macrophage populations, *Proceedings of the Royal Society B* 286 (1904) (2019) 20190730. doi:10.1098/rspb.2019.0730.
- [23] N. Taefehshokr, C. Yin, B. Heit, Rab gtpases in the differential processing of phagocytosed pathogens versus efferocytosed apoptotic cells, *Histol. Histopathol* 36 (2021) 123–135. doi:10.14670/HH-18-252.
- [24] J. Westman, S. Grinstein, P. E. Marques, Phagocytosis of necrotic debris at sites of injury and inflammation, *Frontiers in immunology* 10 (2020) 3030. doi:10.3389/fimmu.2019.03030.
- [25] M. P. Thon, H. Z. Ford, M. W. Gee, M. R. Myerscough, A quantitative model of early atherosclerotic plaques parameterized using in vitro experiments, *Bulletin of mathematical biology* 80 (1) (2018) 175–214. doi:10.1007/s11538-017-0367-1.

- [26] T. A. Angelovich, A. C. Hearps, A. Maisa, T. Kelesidis, A. Jaworowski, Quantification of monocyte transmigration and foam cell formation from individuals with chronic inflammatory conditions, *JoVE (Journal of Visualized Experiments)* (2017) e56293doi:10.3791/56293.
- [27] A. Ghattas, H. R. Griffiths, A. Devitt, G. Y. Lip, E. Shantsila, Monocytes in coronary artery disease and atherosclerosis: where are we now?, *Journal of the American College of Cardiology* 62 (17) (2013) 1541–1551. doi:10.1016/j.jacc.2013.07.043.
- [28] E. Bruckert, D. Rosenbaum, Lowering ldl-cholesterol through diet: potential role in the statin era, *Current opinion in lipidology* 22 (1) (2011) 43–48. doi:10.1097/MOL.0b013e328340b8e7.
- [29] Kummer confluent hypergeometric function, <https://functions.wolfram.com/HypergeometricFunctions/Hypergeometric1F1/>.
- [30] Hermite hypergeometric function, <https://functions.wolfram.com/HypergeometricFunctions/HermiteHGeneral/>.
- [31] Y. Ge, M. Huang, Y.-m. Yao, Efferocytosis and its role in inflammatory disorders, *Frontiers in Cell and Developmental Biology* 10 (2022). doi:10.3389/fcell.2022.839248.
- [32] C. Yin, B. Heit, Cellular responses to the efferocytosis of apoptotic cells, *Frontiers in Immunology* 12 (2021) 631714. doi:10.3389/fimmu.2021.631714.
- [33] L. Chen, J. Zhang, X. Yang, Y. Liu, X. Deng, C. Yu, Lysophosphatidic acid decreased macrophage foam cell migration correlated with downregulation of fucosyltransferase 8 via hnf1 $\alpha$ , *Atherosclerosis* 290 (2019) 19–30. doi:10.1016/j.atherosclerosis.2019.09.001.
- [34] C. S. Robbins, I. Hilgendorf, G. F. Weber, I. Theurl, Y. Iwamoto, J.-L. Figueiredo, R. Gorbato, G. K. Sukhova, L. Gerhardt, D. Smyth, et al., Local proliferation dominates lesional macrophage accumulation in atherosclerosis, *Nature medicine* 19 (9) (2013) 1166–1172. doi:10.1038/nm.3258.

- [35] G. L. Celora, H. M. Byrne, P. Kevrekidis, Spatio-temporal modelling of phenotypic heterogeneity in tumour tissues and its impact on radiotherapy treatment, *Journal of Theoretical Biology* 556 (2023) 111248. doi:10.1016/j.jtbi.2022.111248.
- [36] G. Fiandaca, S. Bernardi, M. Scianna, M. E. Delitala, A phenotype-structured model to reproduce the avascular growth of a tumor and its interaction with the surrounding environment, *Journal of Theoretical Biology* 535 (2022) 110980. doi:10.1016/j.jtbi.2021.110980.
- [37] K. Kim, D. Shim, J. S. Lee, K. Zaitsev, J. W. Williams, K.-W. Kim, M.-Y. Jang, H. Seok Jang, T. J. Yun, S. H. Lee, et al., Transcriptome analysis reveals nonfoamy rather than foamy plaque macrophages are proinflammatory in atherosclerotic murine models, *Circulation research* 123 (10) (2018) 1127–1142. doi:10.1161/CIRCRESAHA.118.312804.